2019

NATURAL PRODUCT INDUCTION IN PENCILLIUM AND HUMAN CASPASE CRYSTALLOGRAPHY

kelly j. mcgrath
University of Montana, Missoula

Let us know how access to this document benefits you.

Recommended Citation

NATURAL PRODUCT INDUCTION IN *PENCILLIUM* AND HUMAN CASPASE

CRYSTALLOGRAPHY

By

KELLY JOHN MCGRATH

B.S. Biochemistry, Montana Tech of the University of Montana,
Butte, Montana, 2014

Master's Thesis

presented in partial fulfillment of the requirements
for the degree of

Master of Sciences
in Pharmaceutical Sciences and Drug Design

The University of Montana
Missoula, MT

December 2018

Approved by:

Scott Whittenburg, Dean of The Graduate School
Graduate School

Dr. Andrea Stierle, Chair
Department of Biomedical Sciences

Dr. Donald Stierle
Department of Biomedical Sciences

Dr. Nicholas Natale
Department of Medicinal Chemistry

Dr. Phillipe Diaz
Department of Medicinal Chemistry

Dr. Nigel Priestley
Department of Chemistry

McGrath, Kelly, M.Sc., Fall, 2018   Major
*Pharmaceutical Sciences
and Drug design*

Chairperson: Dr. Andrea Stierle

Acknowledgments

This work was accomplished with the guidance of Dr. Andrea Stierle, Dr. Donald
Stierle, Dr. T.C. Mou, the Priestley Lab, and the Core facilities at the University of
Montana (crystallography, MassSpec, NMR cores). I would also like to thank the
Biomedical Sciences Department for supporting me and my research for the last 4 years,
and for providing funding for the RapiData workshop in Spring of 2017. These were
fantastic learning opportunities that I simply wouldn't have gotten had I picked a
different department or lab.

Special thanks needs to be made to both Dr. Andrea Stierle and Dr. Donald Stierle
for taking on a graduate student during a time of financial hardship. Funding and
resources were always tight, but access to their expertise was never limited, and that's
also something I don't think I would have gotten in a different lab. Concerning the
Priestley Lab, much of the antibiotic testing would not be accomplished without the
expertise of Jeremy Alverson and the resources provided by Dr. Nigel Priestley. A
similar degree of gratitude is due for Dr. T.C. Mou who how taught me the in's and out's
of protein expression, purification and crystallography, while providing an enjoyable
work and learning environment for me as a visiting graduate student. It's also worth
noting that the completion of this manuscript and my education in whole would not have
been possible without my friends and family, in particular Dr. Margaret Elmer-Dixon at
the University of Montana and (soon to be Dr.) Alexandra Weinheimer at Stoney Brook
University. Both provided much need support and insight throughout the years, and also
helped proof read and edit the ensuing document.

Abstract

The first project discussed was aimed at further expanding on coculture and culture induction techniques in extremophilic fungi under the supervision of Dr. Andrea Stierle and Dr. Donald Stierle. Quantitative testing of crude and purified compounds was accomplished using Alamar Blue Assays through our collaboration with the Priestley Lab at the University of Montana. Qualitative changes were tracked with reverse-phase liquid chromatography-quantitative time of flight (RPLC-QTOF) and proton NMR spectroscopy (^{1}H-NMR) through the Mass Spectroscopy and NMR cores at the University of Montana. The second portion of this thesis deals with the expression, purification, and crystallization of human caspase-1 and human caspase-3 with natural product inhibitors under the supervision of Dr. T.C. Mou with help from the University of Montana crystallography core facility and the Sprang Lab.

These projects aimed to further expand on natural product techniques as they pertain to the discovery of chemical scaffolds with useful antimicrobial and anti-inflammatory activity. This was done through the application of cultutre induction using methanol and protein crystallography.

Table of Contents

Chapter 4. Protein Expression and Crystallography

Tables, and Figures

Chapter 1. Introduction to Drug Discovery

Section 1. Introduction to Natural Products

Introduction to Natural Products

"Natural products are small molecules produced naturally by any organism including primary and secondary metabolites" (https://www.nature.com/subjects/natural-products). Natural products were the first antibiotics, the first anti-inflammatories, and some of the first psychoactive compounds to be used clinically (Dias et al. 2012). While recorded history from these times can be difficult to track, and often delves into the realm of mythology, it is thought that traditional Chinese medicine (TCM) was developed by Shennong around 4,500 years ago, when he compiled the original text "Ben Cao Jing" or "Shen Nong Ben Cao Jing" (translates to "Divine Farmer's Classic of Materia Medica" among numerous other translations). In this text, 365 traditional Chinese medicines are described by their physical appearance, taste, and their effect on the human body. (Foreword to "The Divine Farmer's Materia Medica: A Translation of the Shen Nong Ben Cao" by Shou-Zhong Yang (Editor)). As the process has become more refined, so too has the application of natural products from a more primitive manner (chewing on bark or other useful plants) to the quantitative realm of modern pharmacy (Moloney MF. 1919. Irish ethno-botany and the evolution of medicine in Ireland. Dublin: MH Gill and Son; Bernardini et al. 2017, Stierle et al. 2017, Khalil et al. 2018).

As pharmaceutical science moved into the 19th and 20th century, greater focus was put on the effects of a single compounds isolated from natural sources (Dias et al. 2012; Bernardini et al. 2017; Chen et al. 2018). This would consist of harvesting natural sources of a compound or by fermentation techniques, which are then processed and purified to

yield the active components. This has been exemplified via the discovery of a number of clinically relevant antibiotics including penicillin, erythromycin, and vancomycin (Newman and Cragg 2016; Jakubiec-Krzesniak et al. 2018) and anticancer agents including epothilone and taxol (B da Rocha et al. 2001; Kinghorn et al. 2009; Newman, Grothaus, Cragg 2009).

As the science of natural products chemistry emerged into the modern age, the processes used to culture the organisms with desired chemistry has left much to be desired, resulting in recurring isolation of known compounds along with those deemed pan-assay interfering compounds [pan-assay interference compounds (PAINS) cause false-positive assay signals due to reactivity under assay conditions, including covalent modifications or redox effects, chelation, autofluorescence, or degradation. Invalid metabolic panaceas (IMPS) are compounds that are active against numerous biological/pharmacological endpoints] (Vederac et al. 2009; Whitty 2011).

Given the challenge of identifying new compounds from natural sources, more creative and modern molecular and computational approaches have become popular in the effort to produce novel, bioactive natural products. These include mining for the gene clusters associated with new compounds combined with synthetic biology (Bradley et al. 2016, Biggs et al. 2014, 2016), growing previously cultured organisms together (Stierle et al 2017; Onaka 2017; Khalil et al. 2018), through induction of previously cultured organisms with small molecules (Martin et al. 2011) and biomolecules (Schmidt et al. 2014) or using new culturing techniques (Nichols et al. 2011, Ling et al. 2015). While these techniques vary in technical approach, the end goal is very much the same: producing new compounds or increasing the production of previously low yield compounds. Varied

growth conditions and techniques involving coculture and induction can result in the activation of defense mechanisms without resorting to direct genetic manipulation. These techniques can help impart improved survival by sequestering toxic metabolites or by fighting off competitors and attackers via the production of repressed or under-represented secondary metabolites (Mazid et al. 2011; Roze et al. 2011).

Drug Discovery and Infectious Disease

In recent years, with the rise of multidrug-resistant bacteria and the prevalence of resistance in infectious diseases, there has been a call for novel structures with useful antimicrobial activity, a trend that is even more evident once the ESKAPE pathogens (*Enterococcus faecium*, *Staphylococcus aureus*, *Klebsiella pneumoniae*, *Acinetobacter baumannii*, *Pseudomonas aeruginosa*, and *Enterobacter* species) are considered. These are strains of clinically relevant pathogens that have shown antibiotic resistance in nosocomial infections (Santajit and Endrawattana, 2016). With the danger of antibiotic resistance on the rise, the need for newer antibiotics is becoming more and more imperative. The World Health Organization (WHO) proposes that drug resistance "threatens the effective prevention and treatment of an ever-increasing range of infections caused by bacteria, parasites, viruses, and fungi". (http://www.who.int/news-room/fact-sheets/detail/antimicrobial-resistance; Prestinaci et al, 2015) For therapies to have the utmost longevity of use, novel structures with antibiotic activity are needed to avoid pre-existing resistance mechanisms.

Brief History of Naturally Derived Antibiotics

Natural products chemistry remains a promising pathway to the discovery of novel structures with beneficial antibiotic activity. In reviews published by Newman and Cragg in 2016, it is reported that 60% of drug approvals are based on natural product scaffolds (Newman and Cragg 2008, 2016). This suggests the method of drug discovery from natural products has had a long history of producing new pharmaceuticals. One of the most notable natural products is penicillin produced by the fungus *Penicillium notatum* (now *P. chrysogenum*) and isolated by Alexander Fleming in 1928. This discovery would ignite what we now refer to as the golden age of antibiotics, during which time many other valuable compounds were discovered including streptomycin, the cephalosporins, aminoglycosides, and vancomycin (Davies 2006) This antibiotic boom also produced several Nobel laureates, including Fleming in 1945 (honoring his discovery of penicillin in 1928), Selman Waksman in 1952 for the discovery of streptomycin from *Actinomyces griseus*, a soil bacterium (Schatz et al. 1944; Woodruff 2014), and Robert Woodward in 1965 for his synthesis of a number of natural products, including the clinically relevant macrolide antibiotic erythromycin (Woodward et al. 1981). More recently, Youyou Tu, Satoshi Omura, and William Campbell were awarded a Nobel prize in 2015 for their work in the discovery of artemisinin (a widely used antimalarial), avermectin, and the semisynthesis of ivermectin from avermectin (the cure for river blindness), respectively. Qinghaosu (modern day Artemisinin) is a natural product isolated from Qinghao (sweet wormwood, *Artemisia annua*), which was first described in traditional Chinese medicine as a treatment for malaria. In the early 1970s, Youyou Tu discovered the need for a cold extraction of Qinghao to preserve the peroxide bridge moiety of artemisinin which is

responsible for its activity. She also determined the structure of artemisinin and was involved in conducting the first human clinical trials for artemisinin (Antimalarial Studies on Qinghaosu, 1979; Faurant 2011; Su and Miller, 2015). The case of avermectin and Ivermectin will be discussed in further detail in the next chapter.

Bioassay-Guided Fractionation

Bioassay-guided fractionation provides a rational approach to following activity from a crude extract to a bioactive, purified compound. This process involves extensive testing of crude extracts and the chromatographic fractions produced at each step of the purification process. This process has been employed by the Stierle Lab and several others to yield bioactive compounds in high purity and allows a researcher to effectively track activity from a crude extract down to a purified compound. Until 2016, the primary focus of the Stierle research laboratory has been the isolation of novel compounds that inhibit the enzymes caspase-1, caspase-3, or MMP-3. In the last two years they have also begun looking for compounds with antibiotic activity (Stierle et al 2017).

Caspase-1 has been shown to be up-regulated in pathologies including cancer, autoimmune disease and inflammation (ref.) Caspase-3 is a key enzyme in apoptosis and has been implicated in penumbral damage following stroke, and in the onset of Alzheimer's disease, MMP-3 has been implicated in epithelial mesenchymal transition, a key component of cancer metastasis. These pathologies all represent clinically relevant conditions, to which drug discovery could have a meaningful impact in reducing death and human suffering.

Examples of Biosynthetic Machinery

The production of naturally occurring compounds from an organism can involve any of several quintessential enzyme systems, held under varying degrees of regulatory control. Induction of these pathways can yield higher amounts of previously identified secondary metabolites, as well as novel secondary metabolites not seen under standard growth conditions.

The pathways for generating bioactive structures can often be very complicated in their cascade hierarchy, function, and expression patterns. Additionally, the proteins in these pathways usually originate from more universal biosynthetic pathways, such as steroid synthesis, to produce the corresponding small molecules. These similarities mean many of the precursors, the chemistry involved, and the resulting products share similarity between their native source. For the sake of brevity, two general classes of biosynthetic proteins will be superficially described.

One of the most common classes of biosynthetic machinery is that of the polyketide synthases (PKSs). These enzymes are generally derived from proteins in the fatty acid and steroid synthesis pathways. This class consists of three individual archetypes (I-III), based on the overall assemblage of their active sites. These can be housed on one megasynthase protein (type I), on multiple, physically associated proteins (Type II), or via several individual proteins working in a given syntax (Type III) (Smith et al, 2007).

The nonribosomal peptide synthases (NRPSs) represent a second class of biosynthetic machinery. NRPSs are involved in the synthesis of peptide-like natural products (Daptomycin, Bleomycin) along with cyclic dipeptides called 2,5-diketopiperazines (Cialis/Tadalafil). 2,5-diketopiperazines are the synthetic result of

linking 2 amino acids N-terminus to C-terminus in a 6-member heterocycle containing 2 amide bonds (a 2,5-diketopiperazines) with the sidechains of the associated amino acid precursors (Strieker et al. 2011; Vila-Farres et al. 2017).

These examples are just a small subset of the various ways that cells have repurposed metabolic pathways for small molecule production. However, the field of biosynthetic machinery is immense and is not within the scope of this thesis. Often these sets of biosynthetic machinery are encoded within a cluster of genes which are under control of promoters. These gene clusters often involve regulatory and functional elements that might impart some form of resistance to the producer of said secondary metabolite via expression of catabolic enzymes or efflux proteins. These are referred to as biosynthetic gene clusters (BGCs), the activation of which results in the expression of all necessary elements for secondary metabolite production and regulation. While it is not uncommon for a singular organism's genome to contain several of these BGCs, only a select number of them are expressed under normal laboratory conditions. (Rutledge and Challis, 2015). The classic bacterial operon is regulated by a single promoter for a set of genes. BGCs diverge from this definition in that BGCs are controlled modularly, by several different promoters (Osbourn et al. 2009).

Section 2. Background for Growth and Induction

Impacts of Simple Media and Singular Inoculum

Historically, laboratory cultivation of microbes has focused on singular inoculum and monocultures, a trend dictated by the need for high reproducibility (Stierle et al. 2006,

2007, 2008, 2014). However, culture-induction and coculture techniques have recently been making headway as a means of producing novel secondary metabolites from previously explored microbes (Stierle et al. 2017, Onaka 2017; Khalil et al. 2018). These techniques utilize a phenomenon referred to as cryptic biosynthesis, where key producer-inducer interactions induce the expression of BGCs that would lie dormant under normal laboratory conditions (Nickerson et al 2006; Semighini et al. 2006; Khalil et al. 2014; Wakefield et al. 2017). These gene clusters are generally geared toward the production of host-defense mechanisms, imparting a degree of evolutionary robustness when the target microbe is challenged with competition (Mazid et al. 2011; Roze et al. 2011). This activation can be due to either direct contact, communally shared metabolites, genetic modification, or, hypothetically, a mix of all three. In the case of the berkeleylactones, the Stierles used coculture to induce the production of a series of new small molecules not previously observed in either of the involved strains. Given the nature of Berkeleylactone A, it would seem coculture is inducing the expression of polyketide synthases.

Specific BGCs may be activated through a symbiotic relationship, known as evolutionary pairing, or by exposure to a compound that had previously been a part of the organism's native environment (Rutledge and Challis, 2015; Stierle et al. 2017; Khalil et al. 2018). Sarikaya-Bayram et al. described the role of VeA and other velvet-like proteins in the growth and maturation of fungi and secondary metabolite production. This is thought to be brought about by interactions with LaeA, a methyltransferase capable of regulating secondary metabolism in *Aspergillus* species through activation of metabolic gene clusters (Bok et al. 2004; Hong et al. 2015). This leads to the concept of cryptic biosynthesis, where BGCs can be activated through nontraditional means, such as induction with new culture

media, addition of a small molecule or peptide/biomolecule, or induction in a coculture environment. Additionally, organisms may use autoinduction pathways that rely on the production and accumulation of molecules that trigger changes in gene expression (positively or negatively), which is termed quorum sensing, or by blocking such pathways (quorum quenching) (Nickerson et al. 2006; Semighini et al.). The role of gene expression in secondary metabolite production opens up a number of avenues to access, predict, and stimulate these kinds of interactions, whether from an ecological, biochemical, epigenetic, or bioinformatic stand point.

The Story of Berkeleylactone A

Ecologically-derived induction can involve stimulation with molecules from the organism's native environment (for example, using sulfuric acid to acidify broths) or by utilizing organisms that come from the native environment (coculture; Stierle et al 2017). This represents one of the most obvious approaches for stimulating the production of novel secondary metabolites. The approach of coculture involves taking organisms from the producer strain's native environment (such as a symbiont or a competing organism) and adding it into the culture of the producer strain (Wakefield et al. 2017; Stierle et al 2017; Khalil et al 2018). The production of the novel scaffolds emericellamide A and B were induced in a marine fungus *Emericella* sp. by coculture with a marine actinomycetes, *Salinispora arenicola*.

This methodology was the underlying principle behind the Stierle Lab's discovery of the berkeleylactones. Both were extremophilic *Penicillium* sp. that had been isolated from the surface water of the Berkeley Pit, a mine waste site located in Butte, Montana.

9

The significance of finding life in the water at this location has been noteworthy (Bociaga and Mitman 2003) and has provided the Stierle Lab with a plethora of work over that last 2 decades (Stierle 2008, 2017). In Stierle et al. 2017, the symbiotic relationship between two extremophilic fungi was utilized to produce a series of novel macrolide antibiotics through cryptic biosynthesis. The producer strain used was *Penicillium clavigerum/camimbertii* (designated PW2B) and the inducer strain was *Penicillium fuscum* (designated PW2A). The secondary metabolites produced via coculture included a known compound previously described by Eli-Lily in 1973 (A26771B; Michel et al. 1977), along with several new macrolides named the berkeleylactones (figure 1, Page 13). Michel had also identified a series of compounds labeled A26771A through E, which showed varying degrees of antibiotic activity. These compounds included Gliovictin and hyalodendrin, which had been identified and antiviral and antibiotic (Michel et al 1974). The lead compound, berkeleylactone A shows antibiotic activity against multiple strains of both hospital-acquired and community-acquired MRSAs, *S. pyogenes*, and *B. anthracis*. Conventional macrolide antibiotics are large cyclic structures such as erythromycin, clindamycin, and azithromycin usually assembled from propionate and a number of acetate units into a macrocyclic ester. This results in 14, 15, or 16 membered rings with several points of oxidation along their carbon backbone. Although the berkeleylactones are classified as macrolide antibiotics, they differ from the canonical macrolides (erythromycin, clindamycin, etc.) in two important structural features:

- The berkeleylactones lack the sugar moieties associated with both the antibiotic activity and the induction of bacterial resistance associated with

10

canonical macrolides. This suggests that the macrolides ay have a lower risk of triggering resistance.

- The biosynthesis of berkeleylactone is based on incorporation of polyacetate moieties while that of canonical macrolides is based on polyproprionate moieties,which is exemplified with DEBS synthase, the biosynthetic machinery used to produce a key erythromycin precursor, 6-deoxyerythonolide B (Edwards et al 2014).

The application of extremophilic coculture exemplifies rational methodologies for the activation of previously silent BGCs in the production of new, bioactive secondary metabolites.

The usual mode of action for macrolide antibiotics involves the inhibition of protein synthesis via ribosomal binding, a process not observed with berkeleylactone A (Stierle et al. 2017). Alexander Mankin's Lab at University of Illinois demonstrated that the antibiotic activity of berkeleylactone A is not associated with ribosomal interaction. This suggests that its mechanism of action is unlike that of conventional macrolides. This was done by examining the size protein fragments produced by a ribosome during exposure to a selection of known macrolide antibiotics and berkeleylactone A. This provides information on the target molecule's ability to stall protein production at a given codon or residue number. Stalling of the ribosomal complex results in short peptide sequences that invoke the activity of *erm*, a RNA methyl transferase that modifies an adenine residue in the 23S ribosomal subunit, imparting macrolide resistance and subsequent cell viability (Maravic

11

2004, Arenz et al. 2014) In the case of berkeleylactone A, the full peptide chain was synthesized, suggesting its lack of activity towards the ribosome.

Nutrient and Media-Based Induction

Alternatives to coculture involve induction of an organism's BGCs with small molecules. This involves two general methodologies: (1) providing a substantial amount of precursor for the generation of novel or under-represented secondary metabolites (Ajikumar et al. 2010; Biggs et al. 2014) or (2) induction of BGCs by addition of components to the media that induce the production of new compounds. An inducer could be considered distinct from a component of media in that you would not expect an inducer to be incorporated into the induced product. IPTG would be the classic example, in that it is often used in protein expression as a lac-operon inducer but is not incorporated into the produced protein product (Mittl et al 1997; Martin et al. 2011; Vander-Molen et al. 2013; Vogel et al 2018). Historically, the former has been assessed through direct addition of precursors (e.g. adding farnesol or acetate), or by simply changing the nutrient sources in the media (glucose in media switched to lactose) (Ghorbani-Nasrabadi et al. 2013). This can also be accomplished either by direct modification of the media composition as described previously, or by adding a solvent, such as DMSO, to facilitate uptake of precursors (Li et al. 2012).
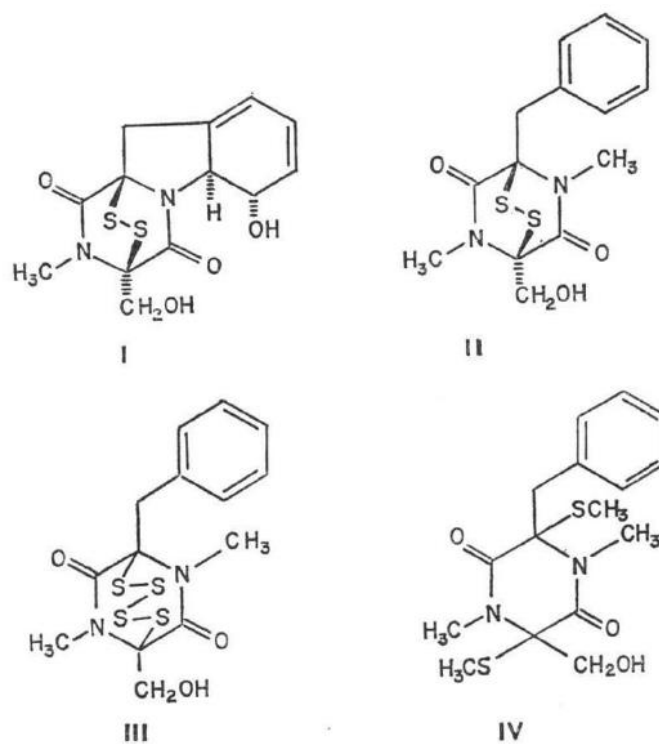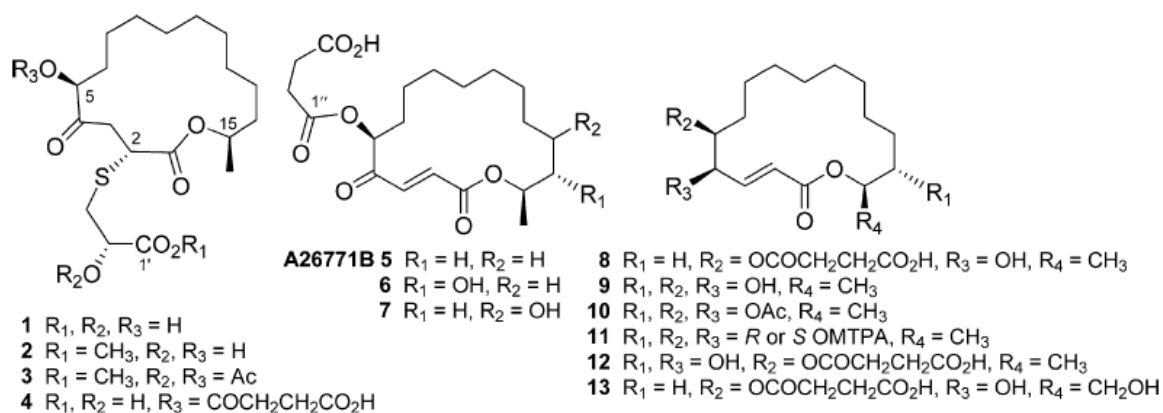
Figure 1. Berkeleylactones and the A26771 series (**Top**) Stuctures of Berkeleylactone series and A26771B (Figure from Stierle et al 2017) (**Bottom**) A26771A (I, Gliotoxin) A26771C (II, S_2-Hyalodenrin) A26771D (III, S_4-Hyalodenrin) A26771E (IV, Gliovictin) (Figure from Michel et al 1973).

These tactics helped modulate the producing strain's access to nutrients - or to specific precursors of desired secondary metabolites - boosting production of secondary metabolites (Biggs et al. 2014, 2016). This may result in either increased production of a secondary metabolite via precursor access, or novel compounds by continued enzymatic action on said secondary metabolite, which might otherwise not be able to reach the cellular location for modification (Yang et al. 2014; Biggs et al. 2014, 2016)

This can be exemplified by the work done by Biggs et al. in 2014 and 2016 where they describe a multivariate modular metabolic engineering (MMME) technique. This process approaches synthetic biology from a module-based paradigm and was applied to the production of taxol, a secondary metabolite of the *Taxus brevifolia*, the Northwest Pacific yew tree, as well as certain fungi, (Stierle et al. 1993) in an engineered *E. coli* strain. This process allowed for tight control of precursor generation, resulting in improved metabolite production over previously employed techniques. This was due to a rate limiting step partway through the synthesis, which resulted in the accumulation of metabolites that were then modified into aberrant compounds not conducive to taxene-5α-ol production. When gene inducers were applied with varying strength (increasing copy number, using different promoters) rate limiting steps could be accounted for, controlling and optimizing the production of the metabolite taxene-5α-ol.

Effects of LPS on Secondary Metabolite Production in Filamentous Fungi

In 2014, Capon et al. examined the effects of induction with LPS on several fungi and bacteria, including a variety of *Penicillium* strains. This research provided insight into a mechanism for inducing the production of secondary metabolites after exposure to cell-

wall constituents associated with gram-negative bacteria. LPS was added to cultures of *Penicillium sp.* at 100 – 0.01 ng/mL and serendipitously resulted in the production of pseurotin analogs (known metabolites of filamentous fungi) and the optical isomer of a known metabolite (-)-rugulosin, along with (+)-deoxyluteoskyrin and (-)-skyrin which had not been previously described in literature.

The effects of LPS in mammalian cells is well understood (Kim et al. 2004). LPS stimulates production of nitric oxide (NO) via inducible nitric oxide synthase iNOS. Schmidt ypothesized that this was also the driving factor behind improved and novel secondary metabolite production in the previously mentioned *Penicillium* species. To examine this hypothesis, light and fluorescence microscopy along with the NO scavenger c-PTIO were employed to examine the effects of induction with LPS on fungal and bacterial cells. These experiments showed that LPS alone induces fluorescence in *Penicillium* sp. (CMB-TF0411), which is quenched when LPS is co-administered with c-PTIO. Strains that were less responsive to induction with LPS in terms of secondary metabolites were also not responsive in the fluorescent microscopy c-PTIO experiments. Schmidt et al. postulated that this is due to the induction of a pseudo-inflammatory state by LPS, akin to what is seen in mammalian cells. Furthermore, they suggest an optimal stimulating concentration of LPS of 0.6 ng/mL for improved production of secondary metabolites in the form of three distinct responses: enhancement, activation, and acceleration. That is, increased yield, novel production, or lowered time of production, respectively.

Chapter 2. Results of Natural Product Experiments

Section 1. General Growth and Induction Experiments

PW2B as the Producing Strain of Berkeleylactone A

The Stierle Research Laboratory had previously identified PW2B (*Penicillium clavigerum/camibertti*) as the producing strain for berkeleylactone A and had also identified the CHCl₃-broth extract of PW2A as being able to induce the production of berkeleylactone A in PW2B (Stierle et al. 2017). Because this demonstrates PW2B's ability to express a diverse array of secondary metabolites, including those with antibiotic activity, it was used as the focus of my small molecule induced growths.

General Growth Protocol

The Stierle Lab has traditionally relied on Potato Dextrose Broth reconstituted with tap water for the growth of their extremophilic fungal strains. This helps provide micronutrients that might not be available in ddH₂O. Growths were conducted in 500mL volumes to detect any initial activity, while providing enough material for the initial steps of purification. Each 1L of culture media was prepared as follows: 20g of complete Potato Dextrose Broth powder (Difco) was reconstituted in 1000 mL room temperature tap water in a 2000 mL large-mouth Erlenmeyer flask. This was then dispensed in 500mL portions into 1L large-mouth Erlenmeyer flasks, the tops were covered in aluminum foil, and the media was autoclaved. Once the media had cooled, it was inoculated with the fungus. The inoculum consisted of a piece of agar (1 – 3 mm²) from a mature 7-day solid culture

(sporulating) of the desired organism. The flask remained stationary for 1 hour to facilitate spore release and dispersal into the liquid medium. After one hour, cultures were grown at room temperature, 180 RPM for 24 hours. At 24 hours, 1 mL of HPLC-grade methanol was added to the inoculated culture media as an inducing agent. This addition utilized aseptic technique via the BSL-2 hood available to the Stierle lab and sterile pipette tips to avoid cross contamination. After induction, the growths were continued at 180 RPM, room temperature for 7 more days before processing.

Bacterial Growths

E. coli (ATCC: 25922) and *S. aureus* (ATCC: 13709) cultures were inoculated from stock solutions provided by the Priestley Lab using aseptic technique in a BSL-2 tissue culture hood. Both *E. coli* and *S. aureus* were grown independently in 5 mL liquid LB (5g NaCl, 5g yeast extract, 10g peptone per 1L DI, autoclaved) cultures and on antibiotic-selective agar plates. Liquid cultures were grown at 37ºC, 120 rpm for 24 hours before use.

PW2B Induction Experiments and Crude Samples

At time of harvest the pH of the broth was measured using litmus paper, and approximately 10 mL of methanol was added to each culture to wet the spores to curtail aerial dispersal during the harvest. Next, the mature culture was gravity-filtered through filter paper, dried for 24 hours and then vacuum dried before a marc-weight was recorded. The filtrate was placed in a separatory funnel and thoroughly extracted with HPLC grade $CHCl_3$ (3X). The resulting $CHCl_3$ extract was dried via rotovap and transferred to a labeled,

tared 1-dram vial using $CHCl_3$. The extract was dried under forced air and then in-vacuo for approximately 1 hour, and its mass (without a cap) was recorded (pg 23).

Section 2. Purification, Characterization, and Activity Testing

Bioassays and Si-flash/HPLC Purification

Disk diffusion assays were conducted to assess initial activity against *S. aureus* and *E. coli*. This was done by loading 20 ug of crude extract dissolved in $CHCl_3$ onto a sterile diffusion disk under a flame umbrella using sterile pipet tips. After drying for approximately 10 minutes near a Bunsen burner to ensure sterility, the disks were placed on agar plates of Difco Antibiotic Medium 2. The plates were incubated at 37°C for 24 hours, at which point zones of inhibition around each disk were marked and measured.

1 mg samples were prepared from both crude broth-$CHCl_3$ extracts and HPLC fractions for antibiotic (Alamar Blue Assays) and protease inhibitor activity bioassays (caspase-1 and 3, mmp-3). The Alamar Blue Assay takes advantage of the REDOX of resazurin, and its ability to be reduced by cofactors such as NADPH, NADH, and cytochromes. These cofactors play crucial roles in cellular respiration, and reduction of resazurin by these cofactors is an indicator of cellular life and viability. The assay was conducted using a micro dilution approach based on Clinical and Laboratory Standards Institute standards for antimicrobial susceptibility (Performance Standards for Antimicrobial Disk and Dilution Susceptibility Tests for Bacteria Isolated From Animals, 5th Edition) utilizing clinically relevant MRSA, *E. coli*, *Candida*, and *Bacillus* strains available to the Priestley Lab.

Crude extracts with antibiotic activity, as identified by Alamar blue results and disk diffusions assays, were further purified using gravity column chromatography utilizing a silica gel stationary phase (Silica gel 60, 0.075 – 0.2 mm, S.A. 470-570 m^2/g; Alfa Aesar). Crude extracts to be purified were dissolved in approximately 1 mL of $CHCl_3$ and loaded onto a hexane-equilibrated Si-flash column. This extract was then eluted with an HPLC-grade isopropyl alcohol (IPA) in HPLC-grade hexane step-wise gradient from 0% -> 100% (0, 5, 10, 20, 30, 50, and 100% IPA in Hex). Samples were collected for each corresponding solvent system. Approximately 1 mg of each crude extract was retained in case any issues arose during screening, or if additional material were needed for follow-up screening assays. Si-flash fractions were transferred to labeled clean 1-dram vials, and each column fraction with a mass > 1 mg was analyzed by [1]H-nuclear magnetic resonance (NMR) in $CDCl_3$ using a Bruker 400 MHz NMR with an autoloader. Further Alamar Blue assays were conducted on Si-flash fractions to determine antibiotic activity. Fractions with activity of ≤ 64 ug/mL against tested strains were subjected to high pressure liquid chromatography (HPLC) using either a methanol/$CHCl_3$ or IPA/Hex stepwise gradient with a silica-gel column (Agilent Technologies Dynamax Microsorb 100-5 Si 10x250mm [DxL]). Pressure was maintained at or around 1,500 psi with a flow rate 2.5-3.5 mL/min while NMR and TLC were used to pool similar fractions. 1 mg samples from pooled-HPLC fractions were also prepared for signal transduction assays and antibiotic testing.

NMR and LC-QTOF analysis

Samples were dissolved in $CDCl_3$ for ^{1}H-NMR and 1 mg/mL samples were prepared in methanol and dispensed into mass spectrometry vials as mandated for use in

the robotic autoloader module for the Agilent Liquid Chromatography-Quantitative Time Of Flight (LC-QTOF) (Mass Spectroscopy Core, University of Montana). This allowed tracking of metabolites between experiments based on the presence or absence of molecular ion peaks corresponding to two previously identified secondary metabolites, gliovictin and hyalodendrin as they were the highest yield in the experiments discussed and had been previously identified in these cultures by the Stierles. For the LC-QTOF, the samples were solubilized in methanol, filtered through cotton, dried, re-massed, and resolubilized in equivalent amounts of methanol. This removed large particulate matter from the crude extracts which may damage the lines or pumps in the machine. This also ensured the final solutions were prepared at 1 mg/mL by accounting for any mass associated with large particulates that were filtered out of solution by the previously mentioned cotton filter. Utilizing a consistent concentration of crude extract for LC-QTOF analysis (1 mg/mL) allowed for relative comparisons of metabolite production between induction experiments. LC-QTOF was run on each crude extract using Stierle's C18 column (Phenomenex Gemini 3 um NX-C18 110Å LC-column 50 x 4.6 mm) on a 0.1% formic acid (Solvent A) to Acetonitrile (Solvent B) gradient in positive mode, utilizing the *DonsLCFAfastposDI.m* method (10uL injection volume, Dual ESI, 350 – 300 $^{\circ}$C gas temp, Fragmentor: 210 V, 0.4 mL/min flow rate, DAD at 214 and 254 nm; 30% B to 100% B from 0 to 12 minutes, 100% B from 12 to 14 minutes, 100% B to 30% B from 14 to 14.1 minutes, 30% B from 14.1 to 15 minutes). MassHunter Qualitative Analysis Software was used to identify weights of known compounds and track changes between experiments. This was accomplished by locating the masses corresponding to previously identified compounds from PW2B and letting the MassHunter software track peaks for those given

masses, while also providing an area for each identified peak. These were then overlaid on the initial LC-QTOF trace, providing a general profile for the tested fraction relative to known compounds. ACD Lab software was used for NMR visualization and peak picking to identify previously isolated compounds from the fractions based on chemical shift patterns characteristic to each metabolite. This was used to help attribute observed activity to compounds previously identified in PW2B that had known antibiotic activity. This was also used to track relative amounts of each known compound in analyzed samples to determine if any given induction technique increased expression of a known compound.

Section 3. Results and Conclusions

Results

Several compounds were used as inducing agents in liquid cultures of PW2B to evaluate their efficacy in the induction of new secondary metabolites production (Table 1, pg 23) Both bacterial lipopolysaccharide and methanol showed the ability to drastically change the secondary metabolome of *P. clavigerum/camibertti* (PW2B) to one that almost exclusively makes 2,5-diketopiperazines, including previously identified compounds gliovictin and hyalodendrin-S$_2$. Of the agents used, it was determined that methanol yielded the best results with the most ease of use and fewest variables. This shows that induction of small molecules can be accomplished in extremophilic fungi. Because of this, the results section will focus on PW2B growths in 500 mL of PDB induced at 24 hours with methanol at a final culture concentration of 0.2%. These growths were done in triplicate, which were then compared to native PW2B cultures using LC-QTOF to access changes in secondary metabolite production as it related to CHCl$_3$ crudes. These compounds were identified

using LC-QTOF (pg 25, 26, 27, 28) followed by 1D NMR techniques (pg 29, 30, 31, 32). Spectra were compared to standards provided by Dr. Donald Stierle who had identified these metabolites from earlier fermentation experiments. Crude samples were compared to samples of purified compounds during my time in the lab of Roquefortine C and Gliovictin/hyalodendrin. These comparisons utilized both LCMS and NMR (pg 28, 32). The production of hyalodendrin-S_2 and hyalodendrin-S_4 was associated with antibiotic activity (pg 24) in the crude fractions, as suggested in Michel et. al. 1973. Gliovictin and hyalodendrin were purified from crude fractions using an equilibrated gravity Si-flash column where the compound elutes in the 5-10% IPA in hexanes fractions, and a means of separating and crystallizing the hyalodendrin's from gliovictin is discussed in detail in the paper by Michel from 1973. Roquefortine was easily isolated from crude fraction samples using an equilibrated gravity Si-flash column where the compound elutes in the 20-30% IPA in hexanes fractions. These two fractions were then pooled, dried, and purified via HPLC on a silica column under 5% methanol in $CHCl_3$ to 10% methanol in $CHCl_3$. Citrinin (a common isolate from PW2B extracts) was not identifiable in LCMS or NMR analysis. Citrinin is associated with a strong peak at 11 minutes utilizing the previously described LCMS protocol (pg 28).

Crude Fractions	Inducer Solutions (final concentrations)	Growth Volume	pH	Crude Mass (g)	Marc Weight (g)
km-1-66A	E. coli in LB (250 uL of OD600 =~0.8)	2x500 mL PDB	n/a	0.0441	13.85
km-1-66D	Autoclaved E. coli in sterile DI (250 uL of OD600 =~0.8)	1x500 mL PDB	n/a	0.0389	11.77
km-2-135B	6 ng/ml LPS in 500uL sterile DI H_2O	2x500 mL PDB	5	0.0013	13.46
km-2-143B	0.6 ng/ml LPS in 500uL sterile DI H_2O	2x500 mL PDB	7	0.0335	13.78
km-2-3A	7.34 uM Asperfuran in MeOH	2x500 mL PDB	5	0.0484	15.16
km-2-3B	30 uM Farnesol in MeOH	2x500 mL PDB	6	0.0529	20.6
km-2-3C	30 uM Indole in MeOH	2x500 mL PDB	5	0.0445	14.85
km-2-39B	1 mL of MeOH per 500 mL	2x500 mL PDB	5	0.0268	14.04
km-3-6A	Control	1x500 mL PDB	5	0.005	9.98
km-3-6B	Control	1x500 mL PDB	5	0.0038	10.26
km-3-7B	1 mL of MeOH per 500 mL	1x500 mL PDB	5	0.0066	9.87
km-3-7C	1 mL of MeOH per 500 mL	1x500 mL PDB	5	0.0057	10.87

Table 1. General Growth Data. Basic growth data for induction experiments with
PW2B. includes fraction names which corresponds to lab notebook number and pages,
inducing agent used and concentration, growth volume and media used, pH of broth
before extraction, mass of dried $CHCl_3$-broth crude, marc weight, and a brief physical
description of each biomass. All of the growth conditions produced beige nitballs.

Compiled Alamar Blue Assay Data

	S. aureus (13709)	S. pyogenes	C. glabrata	B. subtilis	C. albicans	B. anthracis	K. pneumoniae (10031)	P. aeruginosa	E. faecalis	E. coli (25922)	S. aureus (NE277)	S. aureus (PB-2)	S. aureus (PB-3)	S. aureus (PB-6)
KM-1-66A	64	125	250	16	250	>500	>500	>500	125	500	64	32	32	64
KM-1-66D	125	250	25	32	250	500	>500	>500	250	>500	125	32	64	125
KM-2-3A	32	64	64		32	125	250	>500	8	64	16	16	<4	8
KM-2-3B	32	64	64		32	125	250	>500	8	64	16	16	<4	16
KM-2-3C	32	64	64		32	125	250	>500	8	64	16	8	8	16
km-2-39B	32	125	125		125	>500	500	>500	>250	250	32	32	16	64
km-2-135B	125	125	250		125	>500	>500	>500	16	500	64	32	16	125

Denotes that testing is not yet completed

All values are in µM calculated with an assumed MW of 450

Table 2. Alamar Blue Activity Data. Alamar Blue Assay activities for crude fractions tested. All values are depicted in uM concentrations, with an assumed molecular weight of 450 g/mol. Later fractions (km-2-143B, km-3-6let series, km-3-7let series) were not screened as a means of saving time and resources.
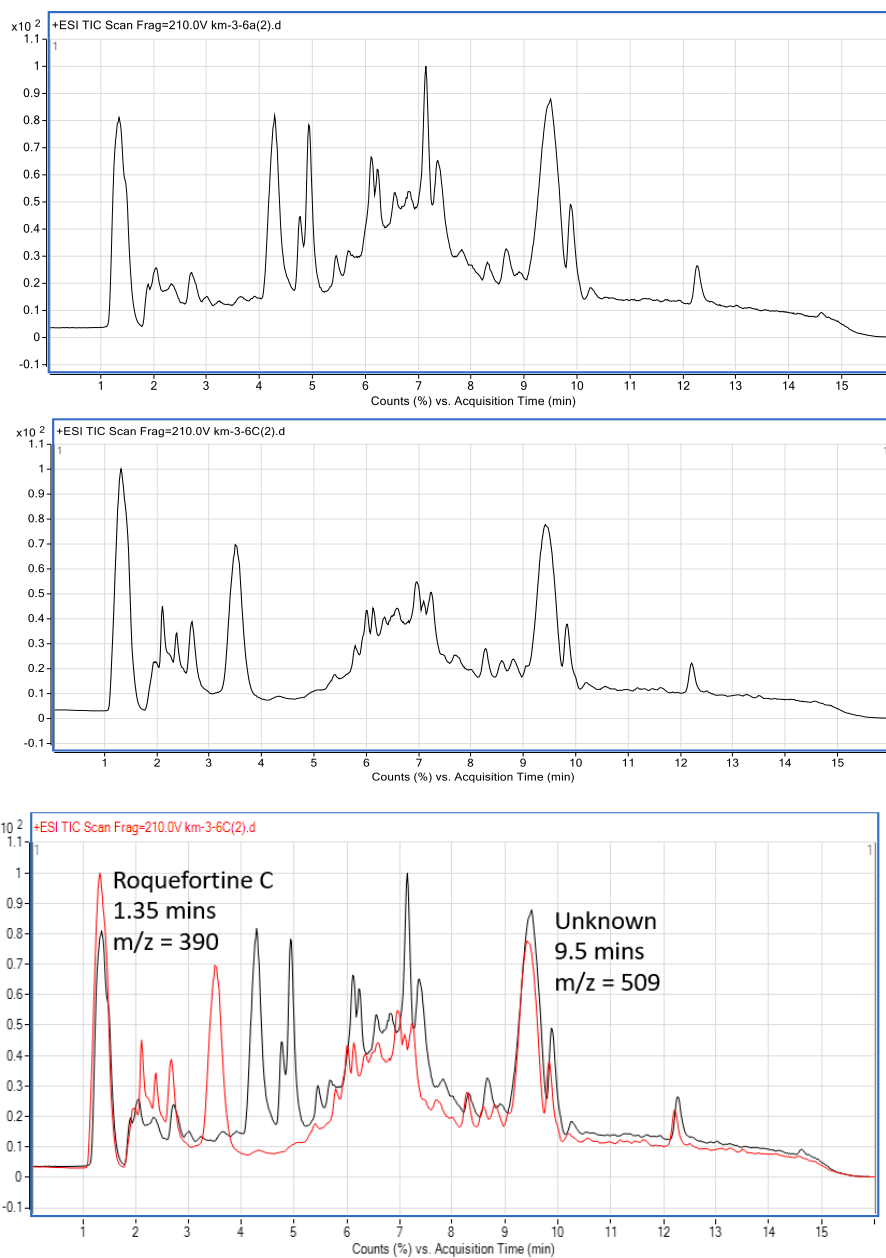
24

Figure 2. RPLC-QTOF Data for Controls. (LC-QTOF) data of CHCl₃-broth crude fractions of PW2B native (control) growths. (**Top**) Km-3-6A (**Middle**) km-3-6C and (**Bottom**) overlay of km-3-6A and km-3-6C. Samples were prepared in HPLC-grade methanol and run on a 30% ACN in 0.1% formic acid to 100% formic acid gradient, utilizing the method DonsLC-FA-fastposDI.m. Files were viewed using Agilent's MassHunter Qualitative Analysis Software Package.

Figure 3. RPLC-QTOF Data for Methanol-Induced Fermentation Experiment. LC-QTOF data of CHCl₃-broth crude fractions of PW2B growths induced with 0.2% Methanol. (**Top**) Km-3-7B (**Middle**) Km-3-7C and (**Bottom**) overlay of km-3-7B with km-3-7C. Samples were prepared in HPLC-grade methanol and run on a 30% ACN in 0.1% formic acid to 100% formic acid gradient, utilizing the method DonsLC-FA-fastposDI.m. Files were viewed using Agilent's MassHunter Qualitative Analysis Software Package.
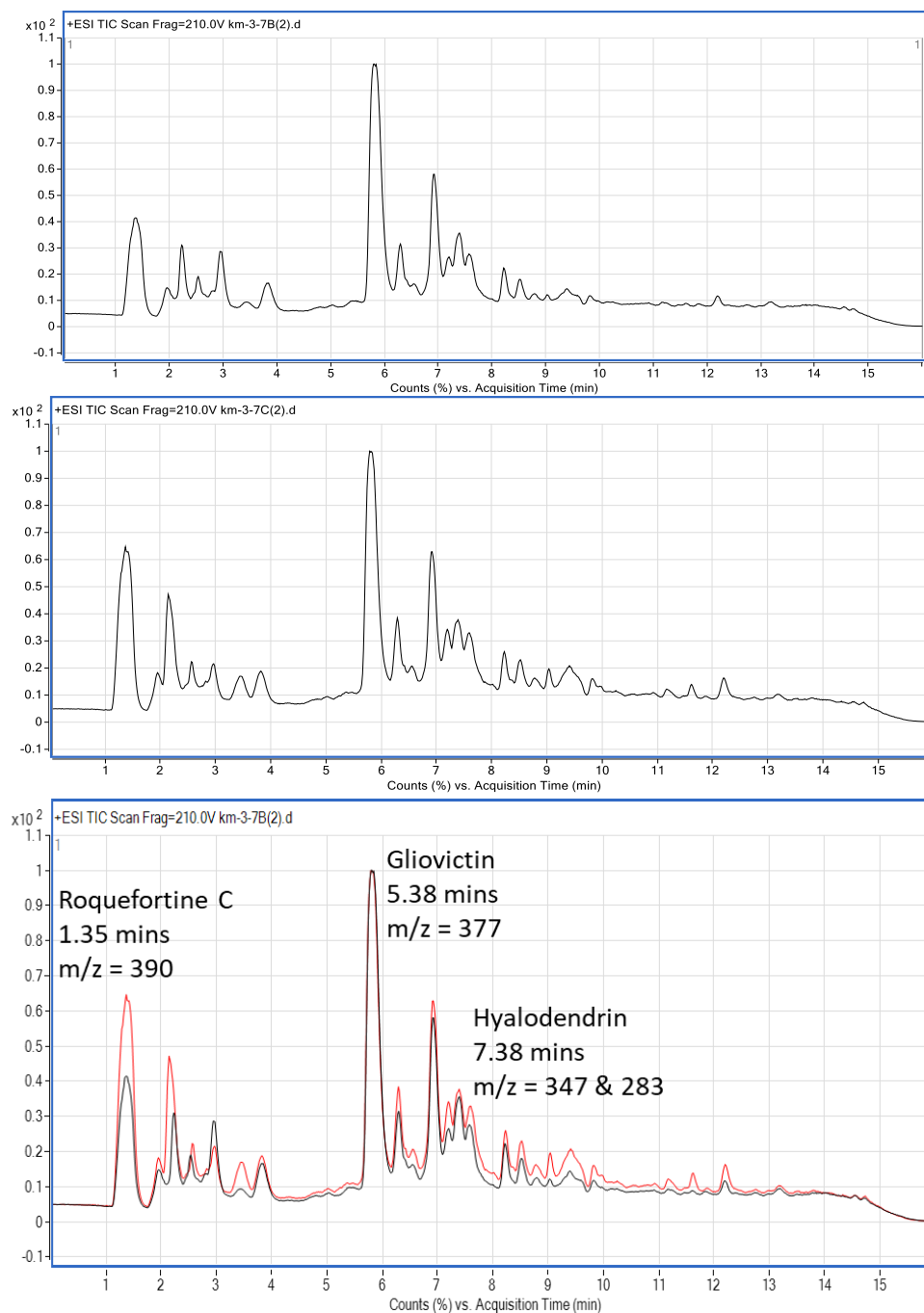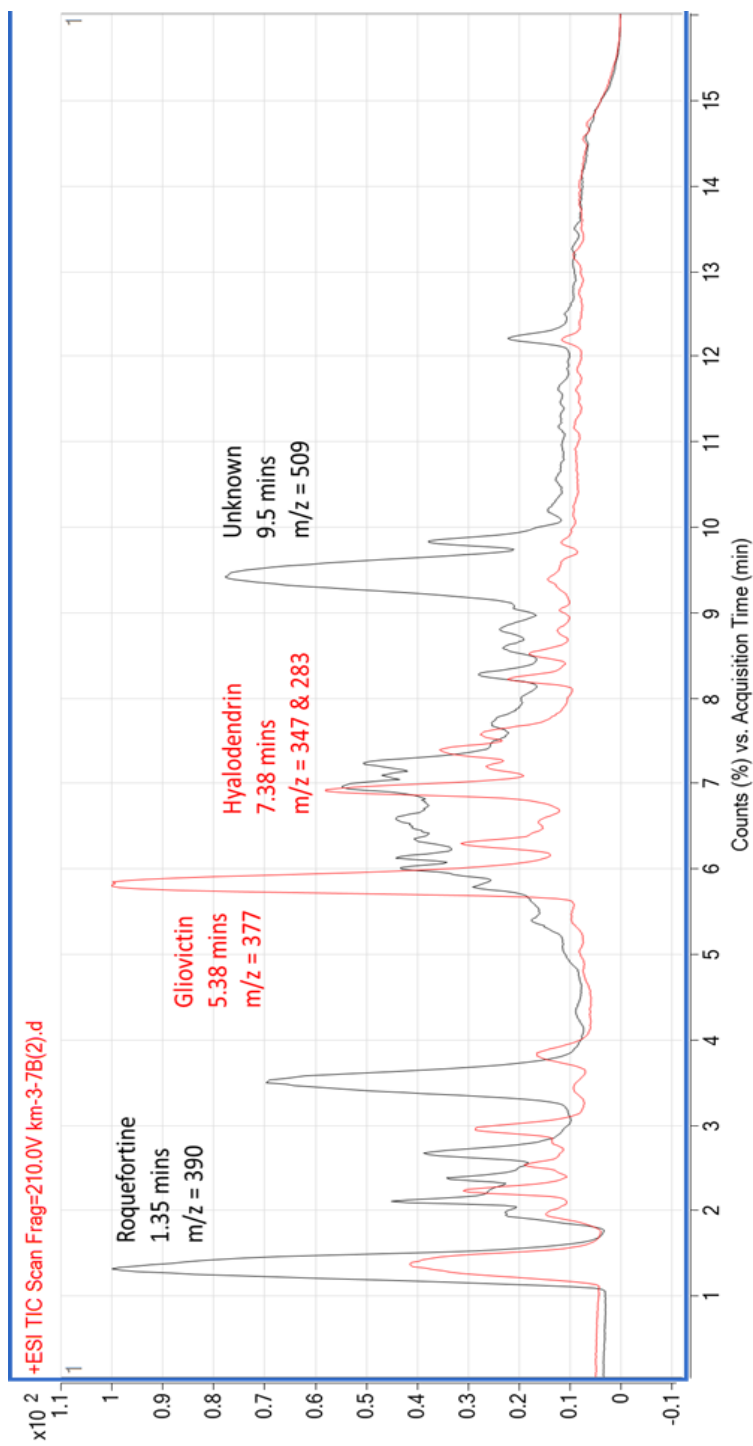
Figure 4. RPLC-QTOF Data for Control vs Induced Fermentation Experiments. (LC-QTOF) data of CHCl₃-broth crude fractions of PW2B naïve growths vs induced with 0.2% HPLC-Grade Methanol. (**Black**) PW2B naïve growth (**Red**) PW2B induced with 0.2% HPLC-Grade Methanol. Samples were prepared in HPLC-grade methanol and ran on a 30% ACN in 0.1% formic acid to 100% formic acid gradient, utilizing the method DonsLC-FA-fastposDI.m. Files were viewed using Agilent's MassHunter Qualitative Analysis Software Package.
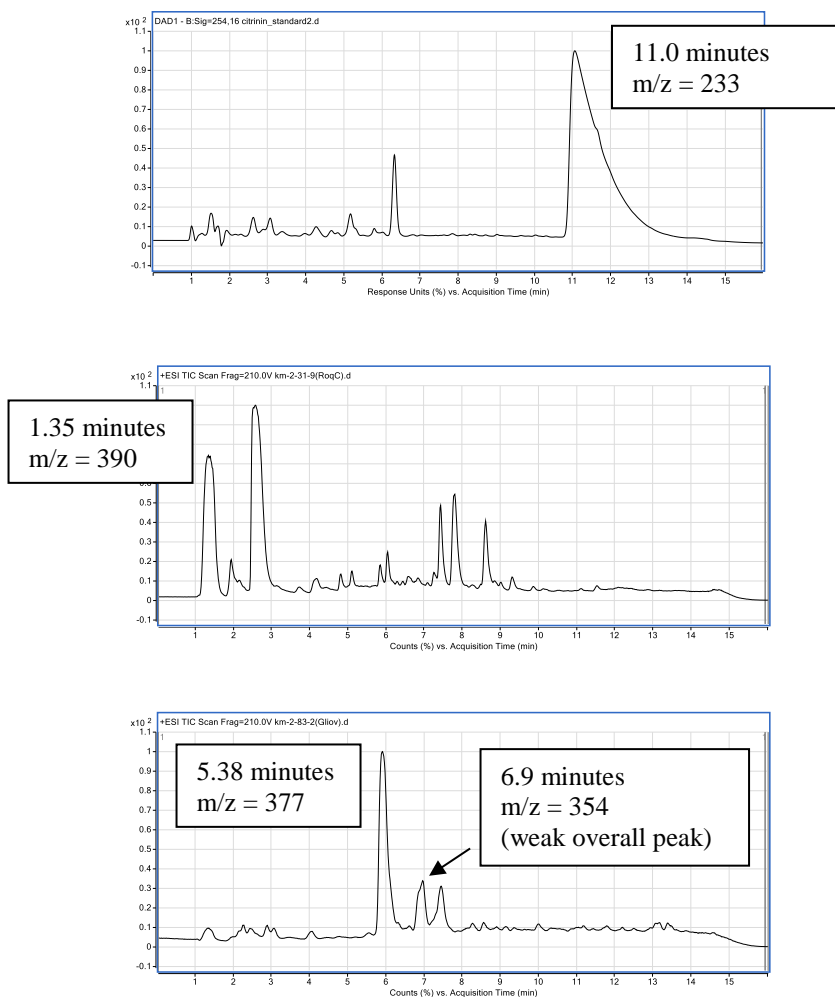
Figure 5. RPLC-QTOF Data for Standards. LC-QTOF data of standards. (**Top**)

Citrinin standard (**Middle Top**) Roquefortine C standard and (**Middle Bottom**)

Gliovictin standard. Samples were prepared in HPLC-grade methanol and run on a 30%

ACN in 0.1% formic acid to 100% formic acid gradient, utilizing the method DonsLC-

FA-fastposDI.m. Files were viewed using Agilent's MassHunter Qualitative Analysis
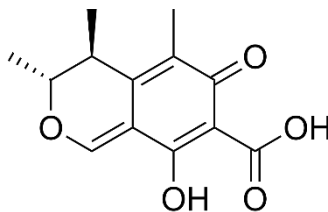
Software Package. (**Bottom**) Structure of Citrinin (https://en.wikipedia.org/wiki/Citrinin)
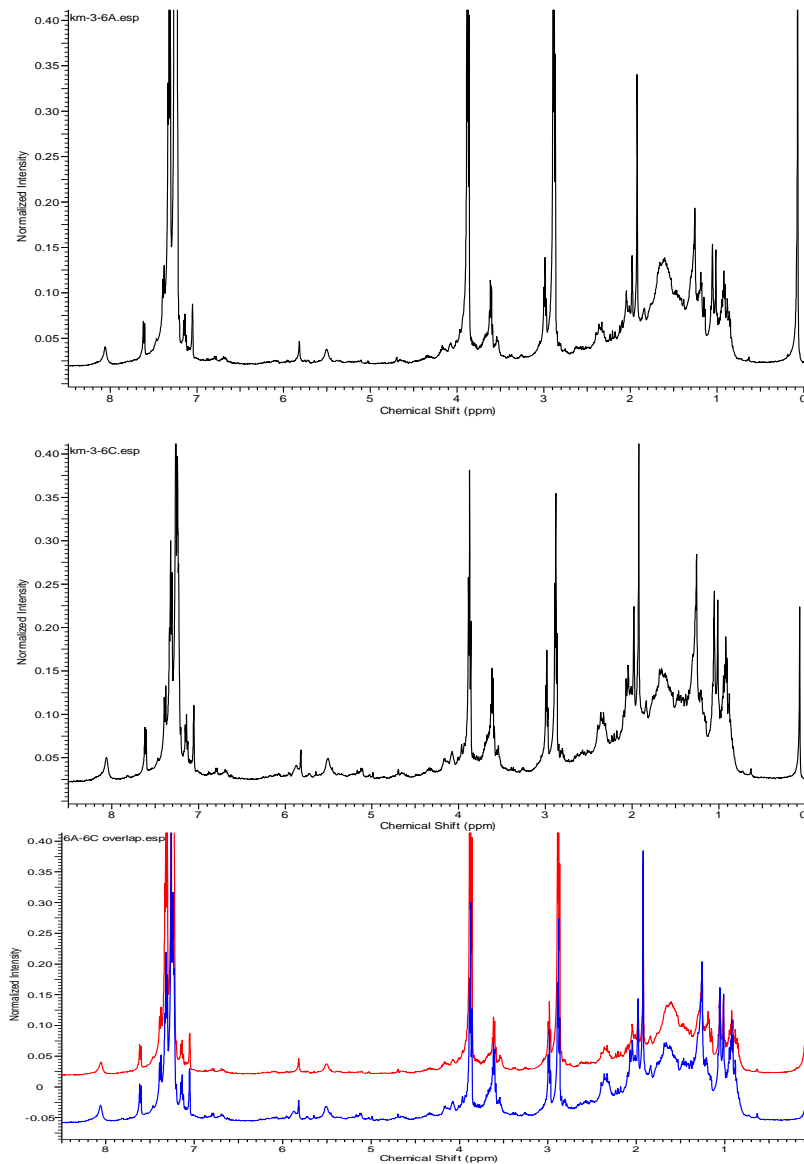
Figure 6. ¹H-NMR Data for Controls ¹H-NMR data of CHCl₃-broth crude fractions for PW2B native (control) growths. (**Top**) Km-3-6A (**Middle**) km-3-6C and (**Bottom**) overlay of Km-3-6let series. Samples were all prepared in 99.8% deuterated chloroform and scanned with a Varian 500MHz NMR. Files were viewed using ACD 1D NMR Processor software.
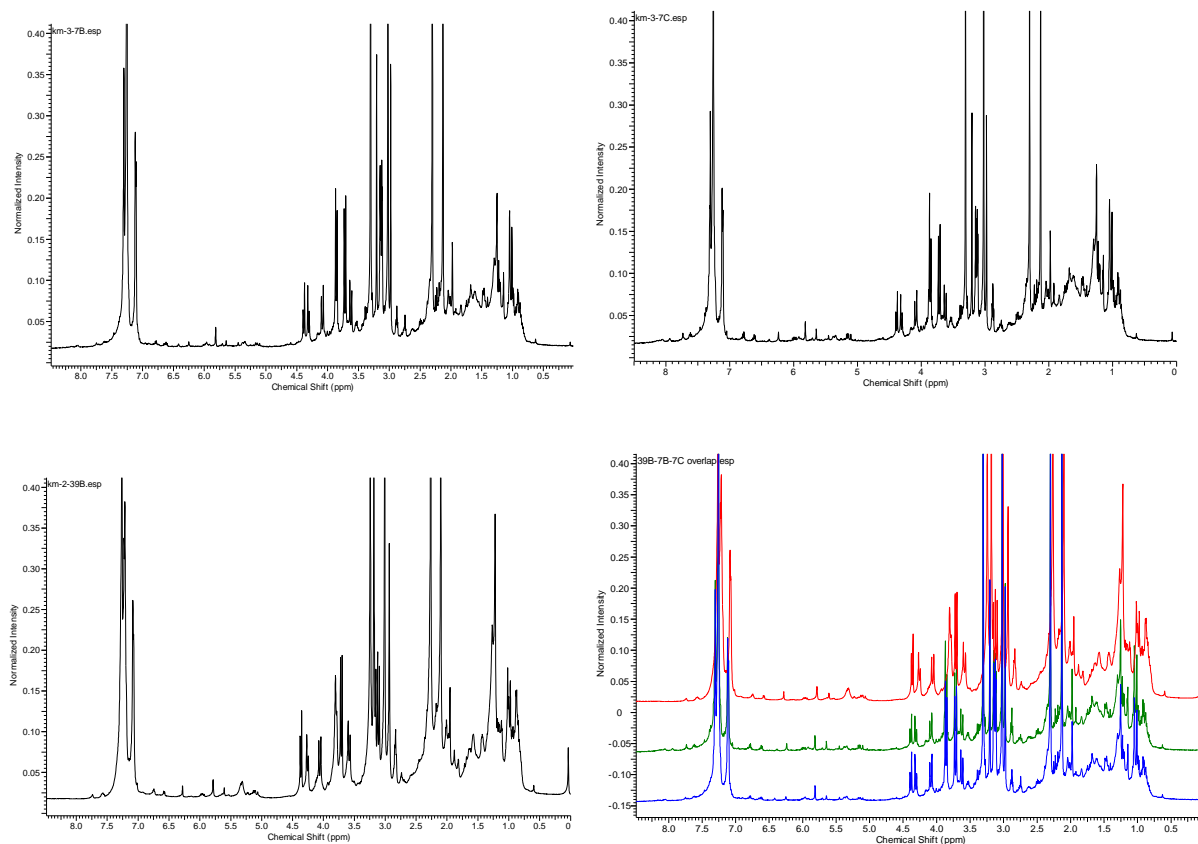
Figure 7. ¹H-NMR Data for Induced. ¹H-NMR data of CHCl₃-crude fractions for PW2B growths induced with 0.2% HPLC-Grade Methanol. (**Top**) Km-3-7B (**Top Middle**) km-3-7C (**Bottom Middle**) km-2-39B and (**Bottom**) overlay of Km-3-67let series and km-2-39B. Samples were all prepared in 99.8% deuterated chloroform and scanned with a Varian 500MHz NMR. Files were viewed using ACD 1D NMR Processor software.
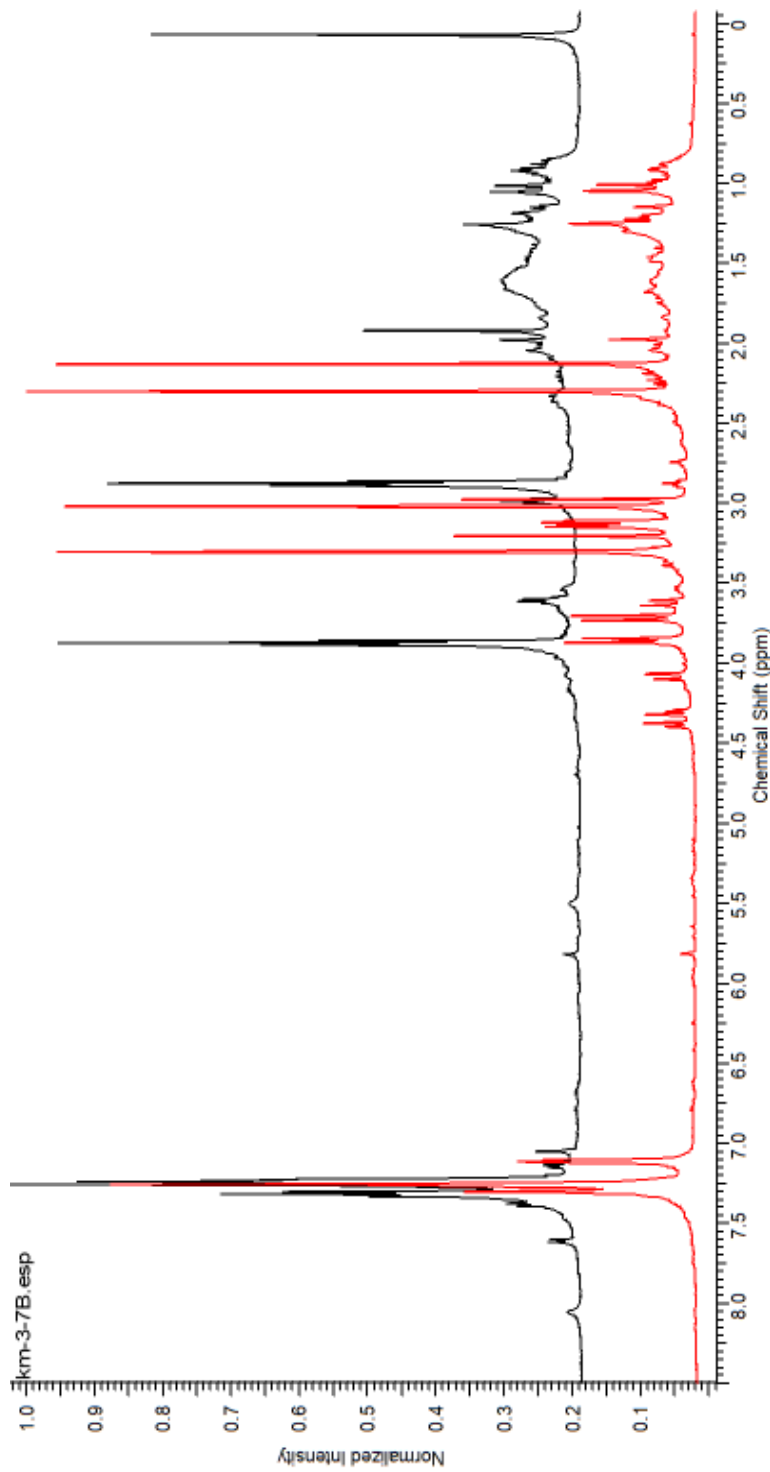
Figure 8. ^{1}H-NMR Data for Control *vs* Induced Experiments. ^{1}H-NMR) data of CHCl$_3$-crude fractions for PW2B grown in PDB vs induced with 0.2% HPLC-Grade Methanol. (**Top**) Control PW2B (**Bottom**) PW2B induced with 0.2% HPLC-Grade Methanol. Samples were all prepared in 99.8% deuterated chloroform and scanned with a Varian 500MHz NMR. Files were viewed using ACD 1D NMR Processor software.

Figure 9. ¹H-NMR Data for Controls¹H-NMR data of standards. (**Top**) Citrinin
standard (**Middle**) Roquefortine C standard and (**Bottom**) Gliovictin standard. Samples
were all prepared in 99.8% deuterated chloroform and scanned with a Varian 500MHz
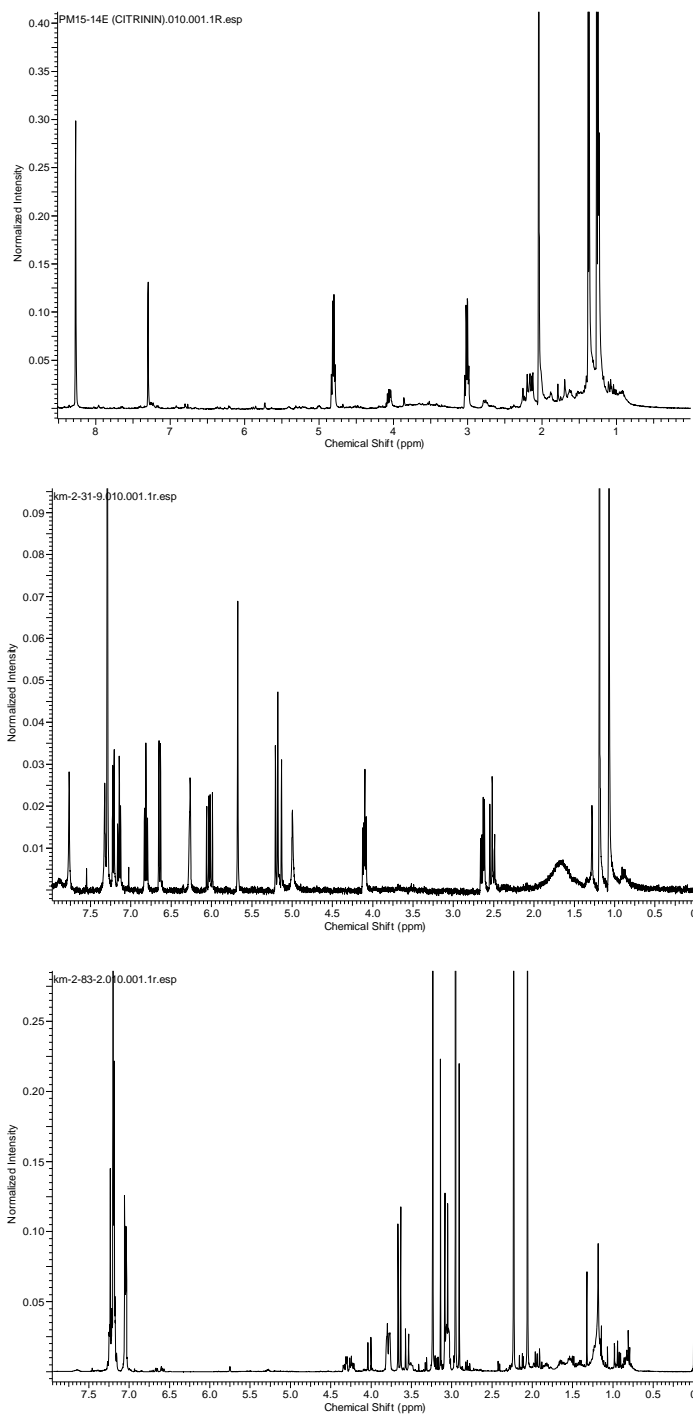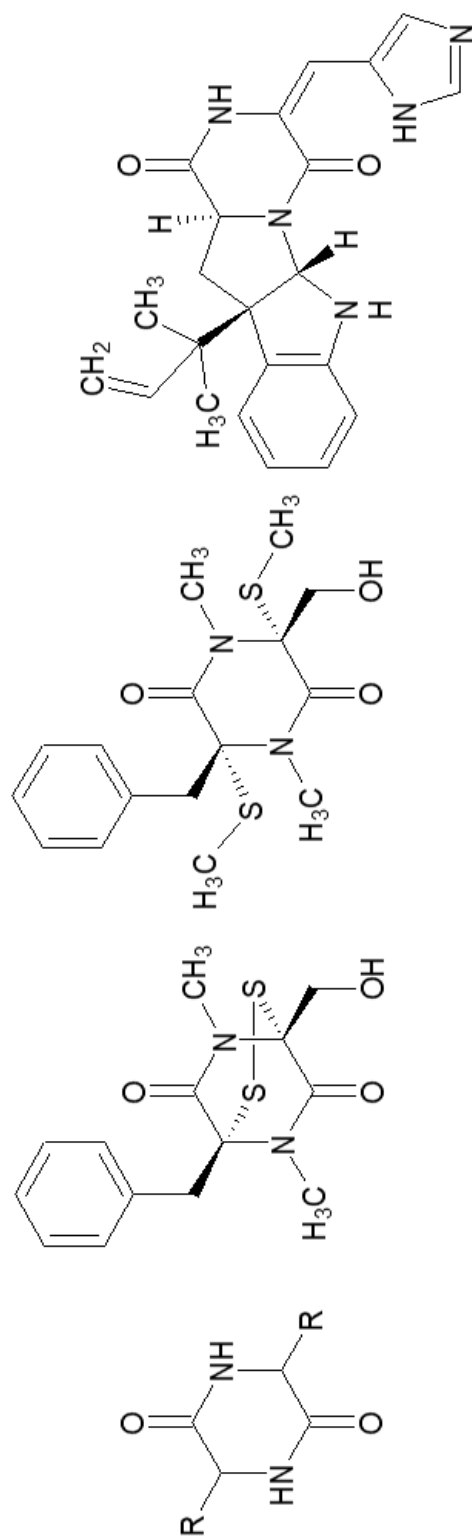NMR. Files were viewed using ACD 1D NMR Processor software.

Figure 10. Structures for Known Compounds. From Left to right: 2,5-DKP core structure, Hyalodendrin-S2, Gliovictin, Roquefortine C. Structures were drawn using ACD ChemSketch Software.

Furthermore, induction with *E. coli* produces a similar secondary metabolite profile to that of growths induced with LPS at either 0.6 ng/mL or 6 ng/mL in Potato Dextrose Broth, where 6 ng/mL proved deleterious to overall secondary metabolite production in PW2B while 0.6 ng/mL showed a more familiar crude mass (pg 23). Indole was also tested as it is the largest yield secondary metabolite from *E. coli,* but these experiments proved inconclusive due to the presence of methanol as a solvent. Later experiments with methanol alone (km-2-39B, km-3-7letter) suggested that this metabolic shift was due to the effects of the solvent, and not the small molecules dissolved in the solvent. This was shown by the km-2-3letter series and the km-3-7 letter series, where each had near identical biological activities despite them all being induced with different small molecules dissolved in methanol (km-2-3letter) or induced with just methanol (km-3-7letter).

In total, methanol induction provided several drastic changes, as evident by LC-QTOF and ^{1}H-NMR analysis (pg 27, 31). For LC-QTOF, induced fractions (7B, 7C) both have a signal at 5.83 minutes with a parent ion at m/z = 377, which represents the M+Na (354+23) adduct for gliovictin. Furthermore, a peak at 7.375 minutes consists of a parent ion peak of m/z = 347 and 283, which represents the M+Na and M-S$_2$+Na peak for hylaodendrin-S$_2$. When these samples were analyzed via NMR, it was apparent that these 2 compounds made up the large majority of the crude fractions for km-3-7B and km-3-7C. Both of these peaks and masses were undetectable in control samples km-3-6A and km-3-6C. It is also worth noting that the control fractions have a peak at 9.50 minutes, corresponding to the mass of an unknown compound with an m/z = 509. All samples also show a peak at 1.35 minutes representing a parent ion of m/z = 390, which was isolated and found to be Roquefortine C.

Conclusions and Future Directions

Growth and induction of P. *clavigerum/camiberti* PW2B with the described methods produced some interesting results. It was successful in that induction with methanol provoked a response that involved drastic, reproducible changes to the secondary metabolome of PW2B. These changes were also associated with antibiotic activity which was ascribed to a series of known 2,5-DKPs, which suggests the induction of BGCs containing NRPSs. Epipolythio-dioxopiperazines (ETPs) are a common class of 2,5-DKP secondary metabolites formed via NRPSs that contain a 2, 4 or 6 sulfur bridge between alpha carbons on the piperazine ring, and include hylaodendrin-S_2, S_4, and gliovictin. In the publication by Gardiner et. Al from 2005, it is noted that epipolythio-dioxopiperazines are capable of general protein inactivation and REDOX cycling. These 2 functions help to fight off competing microbes, potentially reducing the oxidative stress imparted on the producer strain by the environment. This is further exemplified by the broad-spectrum antibiotic activity of hyalodendrin-S_2 and S_4 against gram-positive and gram-negative bacteria and some yeast species.

The impacts of oxidative stress on secondary metabolite production has been previously observed in several publications (Roze et al 2011; Yin et al. 2013). Due to the generalized nature of oxidative stress generation, a generalized response is required from an organism to help control its environment. Furthermore, methanol inducible promoters have been identified in the model organism *Pichia pastoris (*Wang et al. 2016). This alcohol oxidase promoter (P_{AOX1}) is involved in the metabolism of methanol and has been utilized for large scale protein production, like that of the lac operon utilized in Invitrogen's

GATEWAY recombination system. While there is no evidence for the presence of this specific promoter, induction experiments with PW2B and methanol suggests a similar mechanism might be in play for the production of 2,5-DKPs and the expression of NRPSs, specifically for gliovictin and the hyalodendrins.

Future efforts in this project could be directed down a number of routes for verification that induction of non-ribosomal peptide synthases is in fact occurring. This would include sequencing the full PW2B genome. This sequence would then be subjected to any number of bioinformatic programs/approaches to identifying either the appropriate gene cluster (SMURF, antiSMASH, NRPSPredictor, NP.Searcher; Suzuki et al. 2001; Khaldi 2010; Medema et al 2011; Blin et al 2017), focusing on the gliovictin BGC, or for the appropriate promoter (PePPER; de Jong et al 2012), focusing on the P_{AOX1} promoter (Shi et al 2018). The alternative to this would be using strict molecular biology to isolate the DNA of PW2B, and subject it to a number of PCR reactions to try to identify if P_{AOX1} or if a P_{AOX1}-like promoter exists in PW2B.

Chapter 3. Introduction to Protein Crystallography and Drug Design

Section 1. Rational Small Molecule Design

Semisynthetics

While the case for natural products in therapeutics has historically made itself, the need for more potent and safer compounds is always of interest. Also, continued analog development is always of interest to pharmaceutical companies in search for larger drug libraries in the pursuit of continued profits and increased marketability. More recently, this

has been approached utilizing rational drug design. This is exemplified by the acetylation of salicylic acid to acetylsalicylic acid (Aspirin) by Felix Hofmann, which reduced the unpleasant gastrointestinal side effects of salicylic acid when taken orally. Aspirin is therefore classified as a semisyntheti drug, a natural product that was modified to produce an analog with improved activity and/or reduced toxicity. This approach has provided a variety of useful compounds, two of which I will focus on shortly: avermectin analogs and vancomycin analogs. These examples, along with that of aspirin show the utility of combining natural products with rational drug design.

Streptomyces avermitilis was discovered in the early 1970s by Satoshi Omura at the Kitasato University from a soil sample in Tokyo, Japan. Dr. Omura subsequently identified the culture as having antiparasitic activity. After a culture sample was supplied to Dr. William Campbell at Merck in 1973, avermectin was isolated from fermentation broths and identified as the active component. Through derivatization efforts led by William Campbell, Ivermectin was synthesized with lowered toxicity and improved activity via reduction of a single double bond outside of the larger macrocyclic ring. Ivermectin was generated through a trial and error process of generating analogs, screening them in an assay, and then comparing activity profiles of each analog. While this is one of the approaches for rational drug design, there are other routes that have been utilized for analog development.

 (https://www.acs.org/content/acs/en/education/whatischemistry/landmarks/ivermectin-mectizan.html)

If the mechanism of action of a compound is known and well-characterized, then a guided approach to small molecule drug design can be employed, as shown by vancomycin

analog generation. Vancomycin is a clinically used glycoprotein antibiotic whose producing organism was originally identified by Edmund Kornfeld at Eli-Lily in 1953. It was produced by an organism (*Streptomyces orientalis*) isolated from a soil sample from Borneo (Griffith, 1981). Vancomycin works by binding to the incoming NAG-NAM-Peptide sections of the forming cell wall in gram (+) bacteria. Normally, the peptide tails contain 2 terminal D-ala-D-ala residues at a fork in the peptide chain with a repeat of glycine residues that will be clipped during the cell-wall formation process. Vancomycin works by binding these D-ala-D-ala residues via peptide backbone interactions (Schäfer et al. 1996). Resistance to Vancomycin is induced when the terminal D-alanine is converted to D-lactate, eliminating a key hydrogen bond interaction between the amide proton of the alanine and vancomycin itself.

In an attempt to generate analogs that could overcome vancomycin-resistance in pathogenic bacteria, Xie et. al in 2011 developed a series of vancomycin-aglycon [ψ[C(=NH)NH]Tpg^4] analogs that conversely swapped its hydrogen-bond acceptor for a hydrogen-bond donor, to match the backbone change of an amide in D-ala-D-ala (wild type bacteria) to the ester in D-ala-D-lac (resistant bacteria). One of these analogs was reported to have 1000-fold improved potency over vancomycin-resistant enterococcus (*E. faecalis*) and is one of several analogs that attempt to combat the D-ala to D-lac mutant. Although none of these analogs are used clinically, this work demonstrates the utility of applying a structurally-directed approach to drug design from natural products.

These examples illustrate the utility of synthetic modification after the identification of bioactive secondary metabolites. In the case of ivermectin it was an iterative process of making a single modification to a compound and testing the activity of

the resulting analog. Once a sufficient number of analogs were generated and tested, a structure activity relationship (SAR) could be generated for the compound class, and rational drug design could begin.

Vancomycin, on the other hand, represents a much more complicated story due to its 3-dimensional structure that acts as a cap to the peptide-tail target (Sheldrick et al 1996 and Xie et al. 2012, Okana et al 2017). Generating a simple 2D SAR for vancomycin would be significantly less effective in analog design when compared to a 3D representation. This 3D SAR can be assembled using small molecule and protein crystallography which provides detailed information on stable small molecule or ligand-protein conformers. This information can then be used computationally to direct analog development in silico through the application of Monte-Carlos docking simulations (Melvin 2012; Leelananda and Lindert 2016).

History of Protein Crystallography

Protein crystallography with bound ligands allows for an accurate 3D map to be assembled for a ligand and its protein target, which is useful knowledge to have in rational drug design. The history of protein crystallography begins early in the 1900s with the initial discovery that X-rays are diffracted by crystals and by the observations of William Bragg and his son Lawrence Bragg in 1913 (Bragg et al 1913). With the formulation of the Bragg equation, a process was developed to assemble 3D structures from the Bragg reflections, the pattern of dots that are produced on the receiver side of an x-ray diffractor. This allows for spatial and angular measurements to be made between the atoms that produced each Bragg spot. When applied to protein crystals, x-ray diffraction can provide a detailed map

of the target with theoretical resolutions of up to 1 Å. Sir John Kendrew generated the structure of myoglobin, which was the first protein to be crystallized and its structure determined, for which he and Max Peruitz were awarded a Nobel Prize in Chemistry in 1962 (Kendrew et al. 1958). Although this marked the beginning of x-ray crystallography of proteins, the technique would not be used successfully for structure-based drug design until the 1990s where crystal structures were used in modeling (Carrillo et al. 1990, Roberts et al 1990) and in cocrystallization experiments for analog design (Ghosh et al. 2007). These structure-based strategies have been used to identify potential peptide-backbone interactions with HIV protease. This information was then used to modify a compound derived from structure-based drug design (Darunavir; Ghosh 2007; 2015) into even more potent analogs.

There are a number of clinically used small molecules generated through the use of structure-based drug design. As stated by Rob van Montfort and his colleagues in his publication from 2017, "As we write, FBDD (fragment-based drug design [a subset of structure-based drug design]) has yielded over 30 clinical drug candidates and also three FDA-approved drugs in oncology: the BRAF inhibitor vemurafenib, the BCL-2 inhibitor venetoclax, and the CDK4 inhibitor ribociclib." (van Montfort and Workman, 2017). Drugs developed with the assistance of SBDD also include Imantinib (BCR-abl inhibitor), Dorzolamide (carbonic anhydrase inhibitor) and Boceprevir (NS3 protease inhibitor) and Darunavir (HIV protease inhibitor) (Ghosh et al 2007; Murray and Reese, 2009; Howe et al 2013; Jaskolski et al 2014; Blundell 2017; van Montfort and Workman, 2017).

This high definition structural data can be used to help further understand (1) the mechanism of action for a particular ligand, (Suguna et al 1987; Esnouf et al 1995) (2) to

establish a network of interactions responsible for the ligand-protein association, (Mittl et al 1997) (3) provide a negative template for the generation of novel structures (Ghosh et al 2007, 2015; Howe et al 2013), and (4) provide insight into ligand selectivity between two target proteins (Guzik et al. 2017). Structure-based drug design represents a rational way to design higher affinity analogs while providing structural information on important chemical motifs, which relies heavily on protein crystal structures. These 3D structures then can be optimized for either protein binding, for identifying motifs not involved with the protein-ligand interaction, and for SARs to be established (Melvin 2012; Leelananda and Lindert 2016). Structural characteristics can be used for identification of sites for modification to help improve selectivity, reduce toxicity, or improve the pharmacokinetic profile of future analogs (Guzik et al. 2017). While these structures only represent the most stable conformers of the protein and ligand that allow for crystallization, the level of detail provided is unmatched with any non-diffractive technique. This detail can help provide direct information on analog development, as it had with Imantinib, Darunavir, Boceprevir, and other previously mentioned clinically relevant compounds (Murray and Reese, 2009; Howe et al 2013; Jaskolski et al 2014; Zheng et al 2014; Bundell 2017; van Montfort and Workman, 2017).

Section 2. Caspase-1 and -3 in Protein-Based Small Molecule Design:

Caspase-1 and Inflammation

For over twenty years the Stierle research laboratory has utilized the inhibition of specific signaling enzymes as a tool for drug discovery.   They use caspase-1 inhibition assays (Enzo) to guide the isolation of caspase-1 inhibitors from complex fungal extracts. Caspase-1 is an important component of inflammation in mammalian cells, and dysregulated inflammation is associated with many different pathologies. Inflammation is a tightly regulated immunological process mediated by several gene products and physiological cell responses. This initially manifests in the maturation of interleukin-1β (IL-1β) via cleavage by caspase-1. Inflammation is initiated when a macrophage is exposed to a damage or pathogen associated recognition pattern, DAMPs and PAMPs, respectively. These are remnants of either viruses, pathogenic bacteria or dead neighboring cells, and include carbohydrates, LPS, dsDNA, ssDNA, and RNA.

In mammalian cells the initial response leads to the production of pro-caspase-1 and pro-IL-1β. Caspase-1 is cleaved from its p30 zymogen to an active p10/p20 heterodimer and is then assembled into the inflammasome. This macromolecular circular heterotrimer protein complex is similar in structure to the apoptosome with which caspase-3 is involved. Once the inflammasome is assembled, caspase-1 cleaves IL-1β, which exits the cell to further provoke the COX-1/2 mediated part of inflammation.

In theory, if you mitigate the activity of caspase-1 you can block inflammation at the source, which could have implications in autoimmune diseases, pain management, stroke, and cancer (MacKenzie et al. 2010). The Stierle lab has isolated and characterized several caspase-1 inhibitors from Berkeley Pit fungi. These active enzyme inhibitors were

then evaluated in the induced macrophage assay to assess their ability to mitigate production of proinflammatory cytokines in a cell-based reporter system.

Caspase-3 and Apoptosis

The Stierle laboratory also looks for novel small molecule inhibitors of caspase-3 (Stierle et al 2014). Caspases play several roles in apoptosis, with all pathways leading to the activation and action of caspase-3. This includes the intrinsic and extrinsic pathways involving caspase-9 and 8 directly upstream from caspase-3. Like caspase-1, caspase-3 is initially expressed as a p30 zymogen which is cleaved to p13/p17 in vivo by caspases 8 or 9. Caspase-3 is also capable of auto-proteolysis meaning caspase-3 can self-activate itself in vitro when purified. Caspase-3 specifically targets the peptide sequence XAXD-X (Thornberry et. Al 1997) and it's been suggested that caspase-3 has upwards of 600 substrates, indicative of its role in apoptosis.

Elevated levels of caspase-3 have been shown in Alzheimer's disease, autoimmune diseases, and stroke. (Su et al. 2001; Ahmed et al. 2002; Wanger et al. 2011; Fan et al. 2014). Of importance is its role following stroke and traumatic brain injury (Manabat et al. 2003; Fan et al. 2014). Elevated levels in the penumbral region surrounding the infarct zone lead to extensive damage beyond the site of the initial insult. The Stierles also use a caspase-3 inhibition assay to find compound that could mitigate this post-stroke damage.

Given the drastic nature of apoptosis, regulation and dysregulation can play a crucial role in the developing body and in developing tumors. Given the roles of the

caspases in autoimmune disease, development, cancer, and inflammation, both caspase-1 and caspase-3 represent useful targets for the realm of structure-based drug design (MacKenzie et al. 2010).

Section 3. Caspases: Structure

The Caspases: General Structure

The caspase (cysteine-aspartate protease) family of proteins gets its name from its active residue and its target peptide. The caspase family exists as a heterodimer of a large, catalytically active, 20 kDa, p20 subunit and a smaller, 10 kDa, p10 subunit both expressed as a singular procaspase zymogen. Generally, the caspases are approximately 30 kDa, cytosolic proteases consisting of 6 β-sheets surrounded by five α-helices. The caspases utilize a nucleophilic cysteine moiety on the large p20 subunit that attacks an amide carbonyl carbon. The subsequent oxy-anion is stabilized by a neighboring histidine residue in the P1 aspartate binding pocket approximately 6Å away (Fang et al 2006).

The Caspases: Ligand Binding Cleft

While the specific substrates targeted can vary for the 14 identified caspases, the structure of the caspase active site, which is made up of loops 1-4, can be described in some more general terms with respect to the S1 and S2 sites (Fang et al 2006). This is shown graphically in Fig. 2 where Ac-DEVD-CHO (Ligand) is extending from the S1 (right) to the S4 (far left) binding sites on caspase-3. The ligand binding cleft for the caspase family proteins is a long trough shaped pocket capable of stabilizing 4 amino acid residues prior

to cleavage. The S1 binding pocket gives the caspase-family its aspartate-selectivity, while the three remaining sites provide further ligand-sequence selectivity. This pocket is at the p10/p20 interface with the active cysteine at the top and its partner histidine located on the opposite side, approximately 1/3 of the way from the rim of the hole, both of which are on the p20 chain. The S1 hole is approximately 8 Å deep and utilizes an Arginine at its bottom to stabilize the aspartate sidechain on the native ligand. The S2 binding site on the caspases are a generally hydrophobic site that stabilizes lipophilic P2 sidechain of the native ligand (pg 46). For caspase-3, this involves a phenylalanine residue, a tryptophan residue and a tyrosine residue, providing a large hydrophobic pocket for caspase-3 preferred P2 residue, valine.
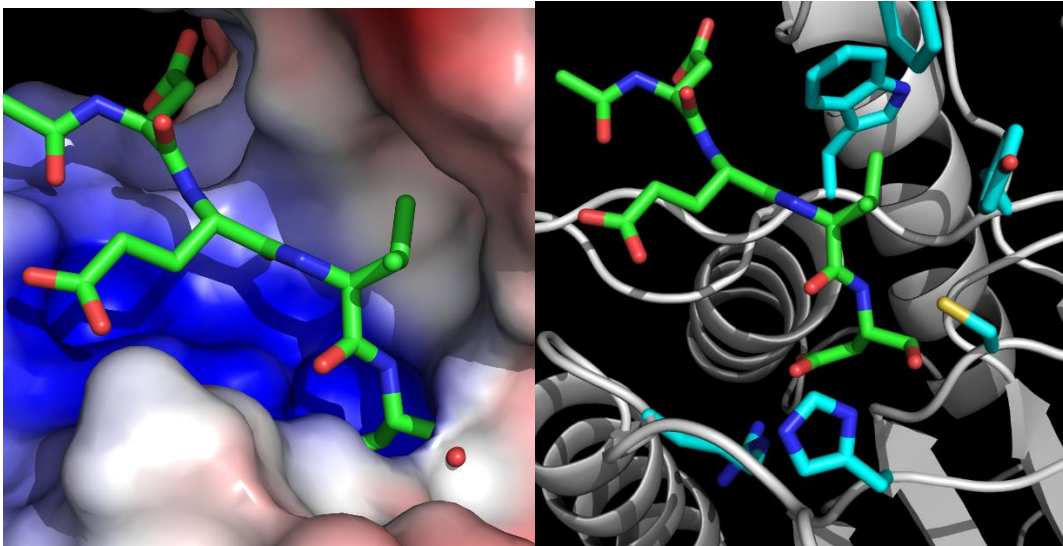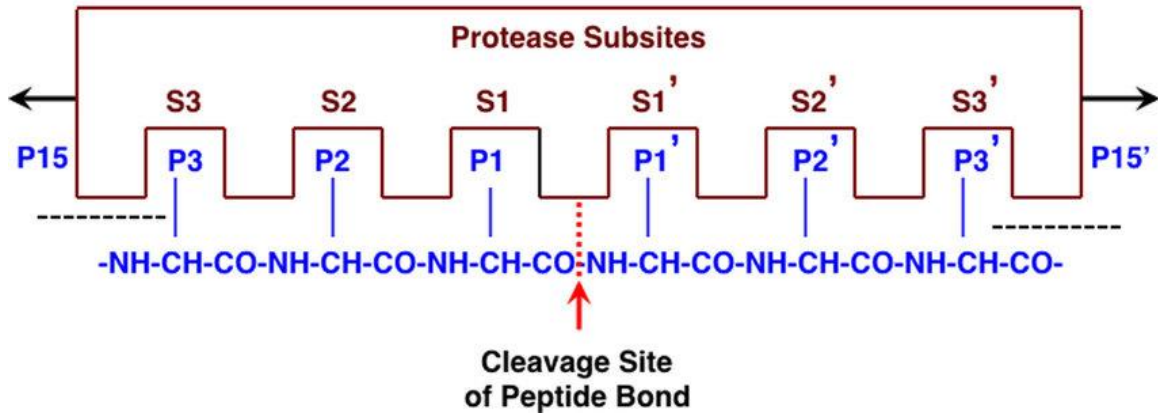
Figure 11. Caspase-3 Crystal Screen Captures. (**Top**) General schematic for protease active sites. (Hook et al. 2015) **(Left)** Image capture of caspase-3 positive control using *Pymol*. Qualitative electrostatic potential map of caspase-3 with a stick model of Ac-DEVD-CHO. This further illustrates the S1 to S4 sites (right to left) represented in loops 1-4. **(Right)** Stick and ribbon representation of caspase-3 S1 and S2 sites bound to Ac-DEVD-CHO. This shows the lipophilic S2 site with the flanking tyrosine, tryptophan, and phenylalanine residues and the charged S1 site with the active cysteine, arginine, and histidine.

Chapter 4. Protein Expression and Crystallography

Section 1. Caspase-1 Methods and Materials

GATEWAY Recombinant Technology and Primer Design

Invitrogen's GATEWAY Recombinant Technology allows for simplistic vectorization and amplification of targeted genes for expression in bacterial, insect, or mammalian cells. This relies on a flanking primer region that gets added to your target DNA sequence via PCR, which is subsequently used to ligate this modified DNA into a species-specific plasmid. This allows for simple protein induction in a variety of cell types, with expression in *E. coli* utilizing a lac promoter which can be induced using iso-propyl thiogylactopyranoside (IPTG).

The process involves 2 classic PCR experiments because the size of the primers involved exceed the suggested limit of around 38 bases. This results in a DNA sequence tagged as designed, with the attB-flanking sequence and any built-in tags on the chosen pDEST vector. The next step involved a BP-clonase reaction where an attB-flanked sequence was transferred into a pDONR donor vector via a protein mixture named BP Clonase. After the BP reaction, the plasmid was amplified using DH5a *E. coli* cells. The final step involved transferring my sequence from the plasmid donor into a vector sequence using a 1-hour LR reaction, similar in nature to the BP reaction. PCR and amplification steps were followed by DNA purification using a QIAprep MINIprep column and the absorbance at 260 nm was used to record the corresponding nucleic acid concentration.

This plasmid was then sequenced, and used to transform BL21 DE3 pLysS *E. coli*, in this case. The transformation protocol is as follows: 50uL of competent cells were placed

47

on ice, to which 4uL of plasmid was added. This solution was incubated on ice for 20 minutes, followed by 45 seconds in a 42°C water bath, and an additional 2 minutes on ice. 450uL of LB was added aseptically to the tube, which was then incubated at 37°C, 180rpm for 1 hour. 100uL of this solution was plated on an Amp+ LB plate overnight at 37°C, and colonies were picked the next day for further processing.

Because the pDEST vectors have Ampicillin and Chloramphenicol resistance sequences and the pDONR provides kanamycin resistance, either can be used for amplification and transformation selection, as appropriate. BL21 DE3 pLysS *E. coli* are super competent *E. coli* engineered to contain both a DE3 lysogen and pLysS plasmids. These plasmids help reduce basal gene expression by utilizing a T7 RNA polymerase (DE3) with a T7 lysozyme (pLysS) and are often employed when the native function of the expressed protein might be toxic or deleterious to cell function. DH5a cells are also a super competent *E. coli* strain used for plasmid amplification.

Caspase-1 Expression and Validation

Based on previously published methodologies (Wilson et al. 1994; Garcia-Calvo et al. 1997; Romanowski et al. 2005; Roschitzki-Voser et al. 2012), caspase-1 was expressed as two independent peptides (p10 and p20) that were combined during refolding experiments after initial purification on a grav-flow Ni-NTA column, relying on the inserted 6xHis tag.

Caspase-1 DNA was ordered from GenScript based on the NCBI reference NM_033292, which was used as the target sequence for BLAST verification after the

GATEWAY LR reactions. This ensured that the target vector was loaded with the target peptide sequence. Caspase-1 p10 and p20 primers were designed based on this sequence with a TEV-protease C-terminal domain and the added GATEWAY flaking sequences as described in the GATEWAY protocol, focusing on residues 307-407 and 120-297, respectively (pg 50). A pDEST17 vector was used which added C-terminal 6xHis tags onto the target peptide directly, which meant that the 6xHis sequence did not need to be designed into the primers.

First, caspase-1 DNA was dissolved in 20uL of DNAase free water. The DNA was amplified via the described transformation procedure using DH5a *E. coli* cells, and subsequently grown on an Ampicillin+ LB agar plate at 37°C. The next day a single colony was picked using aseptic technique and grown overnight in 10mL SOC broth with ampicillin, 37°C, 180 rpm; this was done in duplicate. The following day the 10mL growths were pelleted at 4,000 rpm for 10 minutes. The supernatants were removed, and the pellets were processed using a QIAprep MINIprep kit. Nanodrop was done to validate amplification, with a value at 434.4 and 623.3 ng/uL.

This DNA was then subjected to the GATEWAY recombination process beginning with the PCR#1 protocol for both caspase-1 p10 and p20 independently. The primers, thermocycle runs, and cleaned product concentrations for the caspase-1 GATEWAY protocol are described on the following page.

Caspase-1 p20 Primers (Res 120-297)
Forward Primer #2:
TEV-CASP1-120
5'-**GAA-AAC-TTA-TAT-TTT-CAG-**GGT-AAC-CCA-GCT-ATG-CCC-ACA-TCC-3'
Underlined sections overlap with forward primers.
Flanking region portion is in bold.

Forward Primer #1:
ATTB-TEV
5'-**GGGG-ACA-AGT-TTG-TAC-AAA-AAA-GCA-GGC-TTC-GAA-AAC-TTA-TAT-TTT-CAG-**3'
Flanking region portion is in bold.

Reverse Primer #1 and #2:
ATTB-CASP1-297
5'-**GGGG-AC-CAC-TTT-GTA-CAA-GAA-AGC-TGG-GTC-CTA-**ATC-TTT-AAA-CCA-CAC -3'
Flanking region portion is in bold.

Caspase-1 p10 Primers (Res 317-404)
Forward Primer #1:
TEV-CASP1-317
5'-**GAA-AAC-TTA-TAT-TTT-CAG-GGT**-GCT-ATT-AAG-AAA-GCC-CAC-ATA -3'
Underlined sections overlap with forward primers.
Flanking region portion is in bold.

Forward Primer #2:
ATTB-TEV
5'-**GGGG-ACA-AGT-TTG-TAC-AAA-AAA-GCA-GGC-TTC-GAA-AAC-TTA-TAT-TTT-CAG-**3'
Flanking region portion is in bold.

Reverse Primer #1 and #2:
ATTB-STOP-CASPASE1-404
5'-**GGGG-AC-CAC-TTT-GTA-CAA-GAA-AGC-TGG-GTC-CTA-**ATG-TCC-TGG-GAA-GAG-3'
Flanking region portion is in bold.

Table 3. Caspase-1 Primers. Caspase-1 primers for subunit p20 (residues 120-297) and

p10 (residues 317-404) used in the GATEWAY recombination process. Bold regions

denote flanking attaB sequence. Underlined regions show primer overlap for construct

extension.

DNA amplification:

1. DNA dissolved in 20ul DNAse free water
2. 2 uL added to 50ul of DH5a
3. On ice, 20 minutes
4. 42°C water for 45 seconds
5. Ice for 2 minutes
6. Add 450 ul LB w/o antibiotic
7. 1 hour, 37°C
8. Spread 100ul of cells on amp+ LB plate
9. O/N growth at 37°C
10. Pick into 10 ml SOC o/n 37°C 180rpm
11. Grow ON
12. Miniprep and nanodrop

PCR #1 (flanking region)

1. 1uL DNA (434ng/uL)
2. 1uL fPrimer or f-attb-TEV
3. 1uL rPrimer or r-attb-TEV
4. 1uL dNTP
5. 5uL 10X buffer
6. 41 uL sterile H2O
7. 1uL Taq *add last*
   Spin 30s to mix

PCR #2 (attb-TEV)

1. 1-2uL PCR product (need ~90ng total)
2. 1uL f-attb-TEV
3. 1uL r-attb-TEV
4. 1uL dNTP
5. 5uL 10X buffer
6. 41 uL sterile H2O
7. 1uL Taq *add last*

8. Spin 30s to mix

BP rxn

1. 1-10uL attb PCR product (40-100fmol)
2. 2uL pDONR (150ng/ul)
3. 2uL 5x BP Clonase Rxn Buffer
4. TE buffer pH 8 to total volume of 10uL
5. Incubate 25°C 1 hour
6. Add 2uL of Proteinase K
7. Incubate 10 mins 37°C
8. Transform DH5a on kanamycin+ plates

LR rxn

1. Add volume for 120-160ng BP product
2. Add pDEST vector in equivalence to BP product
3. TE buffer to 6uL
4. 2uL 5x LR clonase *add last*
5. Transform onto DH5a

Thermocycler:

1. 94°C 5 min
2. 94°C 30s
3. 54°C 45s
4. 72°C 2:30
   Repeat 35 times
5. 72°C 10 min
6. 4°C O/N
   Validate w/ nanodrop

Table 4. Transformation Protocol. Protocol for GATEWAY recombination PCR reactions along with thermocycler temperature and reaction times. https://www.thermofisher.com/us/en/home/life-science/cloning/gateway-cloning/gateway-technology.html

The p10 (residues 317-404) and p20 (residues 120-197) plasmids were used to transform two separate batches of BL21 DE3 PLysS cells, which were subsequently grown on Amp+/ LB plates. After overnight incubation at 37°C, single colonies from each plate were picked and used to inoculate separate 50mL LB growths, which were grown at 37°C, 200 RPM overnight. These were used to inoculate two separate 6 x 1L batches of 2xYT (16g Tryptone, 10g Yeast extract, 5g NaCl, pH 7.0) growths containing 100 mg/L Ampicillin (final concentration, added during E. coli inoculation of media), which were then grown at 37°C and 200 RPM for ~4 hours. Log phase growth was tracked using the OD_{600nm} and a spectrophotometer. Once $OD_{600nm} \approx 0.6$, the cultures were induced with 1 mM IPTG (final concentration). Once induced, the culture temperature was dropped to 30°C, and the cells were grown at 30°C 200 RPM, overnight.

The next day, cells were harvested and centrifuged at 7,000 RPM, 4°C, for 35 minutes. The pellets were collected and homogenized with Lysis Buffer (50 mM Tris pH 8.0 and 300 mM NaCl, filtered at 0.2 um) using a hand blender. The homogenate was then centrifuged at 35,000 RPM, 4°C, for 35 minutes. The pellets were then collected and homogenized with Wash Buffer (50 mM Tris pH 8.0, 300 mM NaCl, and 1M Guanidine-HCl, filtered at 0.2 um) using a dounce on ice. The homogenates were again centrifuged at 35,000 RPM, 4°C, for 35 minutes. This washing process was repeated twice.

The pellets were collected and homogenized with Solubilizing Buffer (20 mM DTT and 6M Guanidine-HCl, filtered at 0.2 um). Homogenates were again centrifuged using a floor mounted centrifuge at 35,000 RPM, 4°C, for 35 minutes. The supernatants were collected, and an SDS-PAGE was run to verify the location of p10 or p20, respectfully, in the solubilizing buffer.
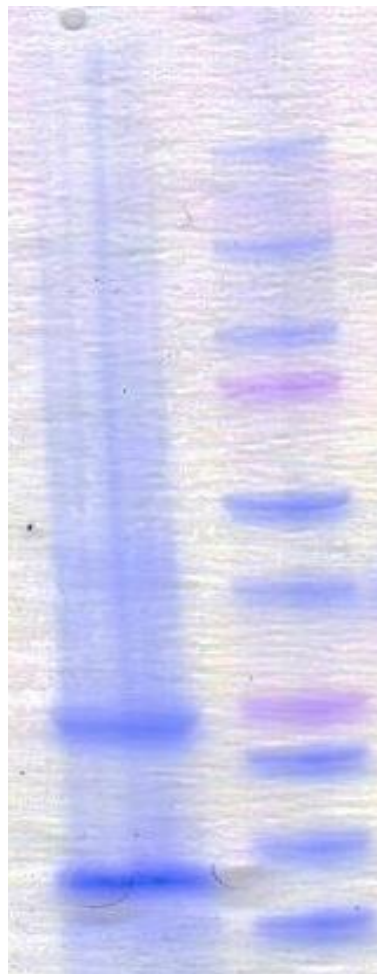
Figure 12. Caspase-1 SDS-PAGE. SDS-PAGE of caspase-1 p10-p20 solution in denaturing buffer. Gel was stained using Coomassie Brilliant Blue. Image depicts bands at approximately 20kDa and 10kDA, along with a kaleidoscope ladder on the right (Biorad).

Caspase-1 Refolding

Because caspase-1 subunits are expressed in insoluble-inclusion bodies, denaturation of the subunits was conducted independently and subsequent refolding experiments were conducted on the subunits in a 2:1 p10:p20 ratio by volume, respectively. This approach employed methodologies that had been previously reported for caspase-1 refolding (Scheer and Romanowski et Al. 2004, pg 55).

The p10 and p20 subunits in Solubilizing Buffer were concentrated to ~4 mg/mL and mixed in a 2:1 ratio by volume. 1 mL of the mixture was added to 50 mL Refolding Buffer (50 mM HEPEs pH 8.0, 100 mM NaCl, 1 M NDSB-201, and 20 mM DTT, filtered at 0.2 um) by several methods as listed on the next page. Rapid dilution entails adding the 2:1 mixture directly to the refolding mixture, bag dialysis employs bag dialysis tubing, while a Slide-a-lyzer is a specific dialysis tool involving a cassette and a dialysis membrane, which is floated in dialysis buffer. In general, this mixture was stirred for 3-8 hours at 4°C or room temperature and then centrifuged using a floor mounted centrifuge at 35,000 RPM, 4°C, for 35 minutes. Visual inspection for precipitate before centrifugation and nanodrop assays after centrifugation were used to quantitate any soluble protein after refolding.

Method	Refolding Buffer	Publication
Rapid Dilution, RT, 4 hours	50mM HEPEs pH 8, 100mM NaCl, 20mM DTT, 1M NDSB-201, 100mM Sodium Malonate	Romanowski et Al., 2004 Garcia-Calvo et Al. 1999
Rapid Dilution, 4°C, 8 hours	50mM HEPEs pH 8, 100mM NaCl, 20mM DTT, 1M NDSB-201	Romanowski et Al., 2004
Rapid Dilution, 4°C, 4 hours	50mM HEPEs pH 8, 100mM NaCl, 20mM DTT, 1M NDSB-201	Modified Romanowski et Al., 2004
Rapid Dilution, RT, 8 hours	50mM HEPEs pH 8, 100mM NaCl, 20mM DTT, 0.1 to 1.0% NP-40	Modified Rano et Al. 1997
Rapid Dilution, RT, 8 hours	50mM HEPEs pH 8, 100mM NaCl, 20mM DTT, 0.05 to 0.2% CHAPs	Rano et Al., 1997
Slide-a-lyzer, RT, 4 hours	50mM HEPEs pH 8, 100mM NaCl, 20mM DTT, 1M NDSB-201	Modified Romanowski et Al., 2004
Bag Dialysis, 4°C, 8 hours	50mM HEPEs pH 8, 100mM NaCl, 20mM DTT, 1M NDSB-201	Modified Romanowski et Al., 2004
Bag Dialysis, 4°C, 8 hours	50mM Sodium Acetate pH 5.9, 100mM NaCl, 15% glycerol, 4 mM DTT	Roschitzki-Voser, Grutter, et Al., 2012

Table 5. Caspase-1 Refolding Conditions. Refolding conditions explored for caspase-1 p10-p20 solution. Progress was followed using nanodrop and SDS-PAGE. Includes publications that provided references for refolding conditions, and if they were modified or not.

Conclusions and Future Directions

Protein refolding represents an extremely complicated process, to which a solution may not be trivial. While I was able to explore several techniques that had previously been published for the refolding of caspase-1 subunits together to form an active caspase-1 heterodimer, none of them proved successful. These included changing the buffer solutions and the dialysis hardware involved during the refolding process, along with extended purification techniques to further improve the quality of the samples to be refolded. The best insight I can offer is on the syntax of buffer addition, whether it is protein added to buffer or buffer added to protein. This syntax can change the refolding landscape by having drastic variations on protein concentration or buffer concentration in the initial moments of the refolding process. Further exploration of this process can be done by employing a burette to slowly add protein or buffer over the course of an experiment. Other examples may include higher volumes of buffer utilizing inexpensive inhibition via malonate, further exploration of dialysis hardware, or utilizing mammalian cells to produce active caspase-1, sidestepping the refolding process entirely (Yamaguchi and Miyazaki 2014)

Section 2. Caspase-3 Methods and Materials

Caspase-3 Expression

Based on previously published methodologies (Denault et. Al. 2002; Romanowski et. Al 2005; Fang et. Al 2006), caspase-3 was expressed as a single peptide that utilized caspase-3's autoproteolytic activity for activation during the purification steps. Caspase-3 was expressed in a manner similar to that previously described for caspase-1. DNA for

NCBI reference NM_032991.2 was ordered from GenScript and was used as the target sequence for BLAST verification after the GATEWAY LR reactions.

Procaspase-3 primers were designed based on this sequence with the GATEWAY flanking sequence and a C-terminal 6xHis tag, focusing on residues 150-401, respectively (pg 58). The DNA sequence was amplified and processed in a similar manner to the caspase-1 DNA utilizing DH5a *E. coli* cells. The PCR products were cleaned after each step using a QIAprep MINIprep column, followed by nanodrop (microvolume spectrophotometer) to access nucleic acid concentrations. This was then used for the GATEWAY protocol as described earlier. The corresponding procaspase-3 plasmid was used to transform BL21 DE3 pLysS using the growth and purification protocol described previously.

The procaspase-3 zymogen plasmid was used to transform BL21 DE3 PLysS cells, which were subsequently grown on Amp+/ LB plates. After overnight incubation at 37°C, single colonies from each plate were picked and used to inoculate 30mL LB growths, which were grown at 37°C, 200 RPM overnight. 5ml of these growths were used to inoculate each liter of a 6x 1L Amp+/2xYT growth (prepared as described earlier), which were then grown at 37°C and 200 RPM for ~4 hours. Log phase growth was tracked using the OD_{600nm}. Once $OD_{600nm} \approx 0.8$, the cultures are induced with 200 uM IPTG (final concentration). Once induced, the culture temperature was dropped to 25°C, and the cells were grown at 25°C, 200 RPM, for 4 more hours.

Cells were then harvested and centrifuged at 7,000 RPM, 4°C, for 35 minutes. The pellets were collected and 12g of pellet was homogenized with 100 mL of Lysis

Caspase-3 Primer with C-terminal fusion 6xHis-tag (Res 150-401)
Forward Primer #1:
ATTB-CASP3-150
5'-**GGC-TTC-GAA-GGA-GAT**-AGA-ACC-*ATG*-GAG-AAC-ACT-GAA-AAC-3'
Underlined sections overlap with forward primers.
Flanking region portion is in bold.

Forward Primer #2:
ATTB
5'-**GGGG-ACA-AGT-TTG-TAC-AAA-AAA-GCA-GGC-TTC-GAA-GGA-GAT**-3'
Flanking region portion is in bold.

Reverse Primer #1:
CASPASE3-401
5'-CTA-GTG-ATG-GTG-ATG-GTG-ATG-GTG-ATA-AAA-ATA-GAG-TTC-TTT-
TGT-3'
Underlined section overlaps with reverse primers.

Reverse Primer #2:
ATTB-STOP-CASPASE3-401
5'-**GGGG-AC-CAC-TTT-GTA-CAA-GAA-AGC-TGG-GTC-***CTA*-GTG-ATG-GTG-
ATG-GTG-ATG-3'
Flanking region portion is in bold.   5'-CAT-CAC-3'
Underlined is stop codon and His-tag repeat   3'-GTA-GTG-5'

Table 6. Capase-3 Primers. Human caspase-3 zymogen primers (residues 150-401) used

in the GATEWAY recombination process. Bold regions denote flanking attaB sequence.

Underlined regions show primer overlap for construct extension.

Buffer (50 mM Tris pH 8.0 and 50 mM NaCl, filtered at 0.2 um) using a sonicator for 4 minutes total, 0.5 seconds on, 0.5 seconds off. The homogenate was then centrifuged at 35,000 RPM, 4°C, for 35 minutes and the supernatant was filtered on a 0.2um filter.

Caspase-3 Purification and Validation

The protein was purified using a gravity-flow Ni-NTA column, utilizing the 6xHis N-terminal tag on pro-caspase-3 provided by the pDEST14 vector. 35 mL of lysate was added to a 5mL Ni-NTA column previously washed with 200 mL MilliQ H_2O. The lysate doped column was incubated for 1 hour with shaking at 4°C. The column was washed twice with 50 mL Wash Buffer (50 mM Tris-HCL pH 8.0, 500 mM NaCl, 20 mM imidazole pH 8.0, filtered at 0.2 um) and once with 45 mL of Elution Buffer (50 mM Tris-HCL pH 8.0, 150 mM NaCl, 250 mM imidazole pH 8.0, filtered at 0.2 um). At this point, the p17/p12 bands are both present due to auto-proteolysis on the Ni-NTA column (pg 60).

The caspase-3 containing samples previously validated via SDS-PAGE were pooled, and further purification was conducted (Fang et al. 2006). A sample was also collected to qualitatively validate capase-3 activity using the Caspase-3 Drug Discovery Kit (Enzo Life Sciences), a fluorometric assay that uses Ac-DEVD-AMC as a fluorogenic substrate (Denault et l. 2002, pg 61). Assays were conducted on 1000-fold dilution of Ni-NTA columns in a black walled, clear bottom 96-well plate. The assay buffer contained 150 mM PIPES pH 7, 50 mM NaCl, 20% sucrose, 0.2% CHAPS, 2 mM EDTA, and 20 mM DTT that was added fresh prior to each assay.
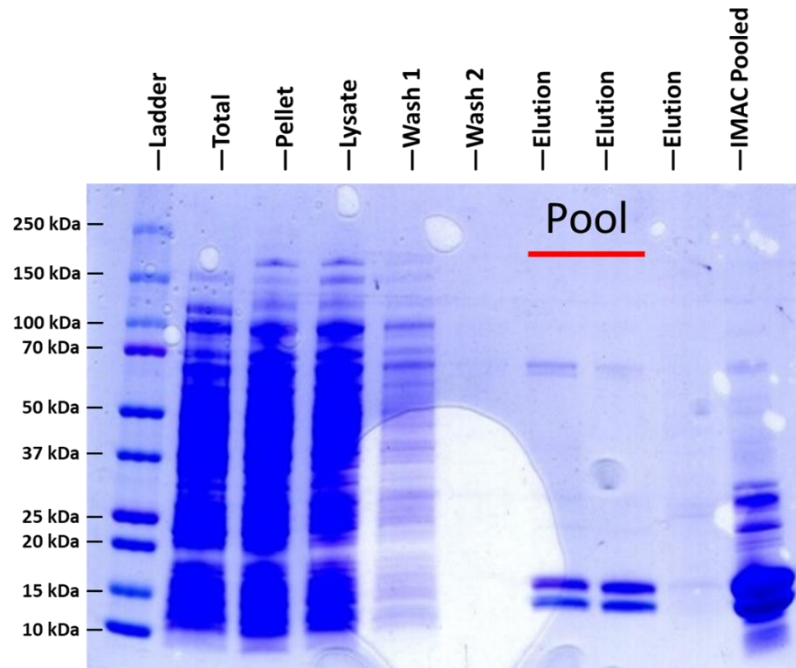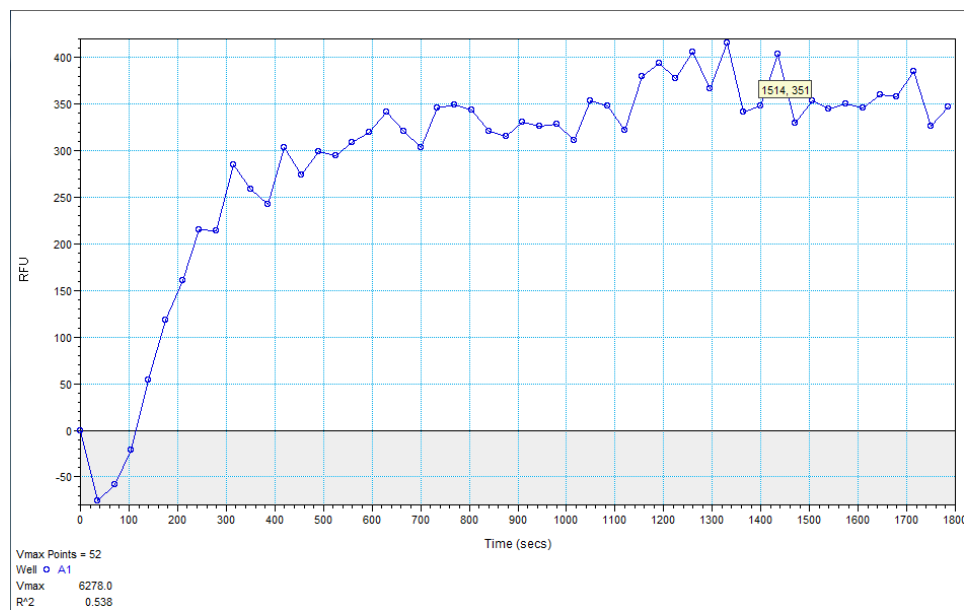
Figure 13. Caspase-3 Ni-NTA SDS-PAGE. SDS-PAGE gel of caspase-3 after grav-flow Ni-NTA purification and zymogen cleavage on Ni-NTA column. Lanes 2 through 5 show crude pellet bands, lanes 7 and 8 show purified, cleaved caspase-3. Gel was stained using Coomassie Brilliant Blue.

Well	2x Buffer	1000x Sample	1x Sample	MilliQ	Ac-DEVD-AMC	Ac-DEVD-CHO	Small Molecule
1000x Assay	50 µL	30 µL	--	--	20 µL	--	--
1x Assay	50 µL	--	30 µL	--	20 µL	--	--
Inhibitor	40 µL	30 µL	--	--	20 µL	10 µL	--
Competition	49-40 µL	30 µL	--	--	20 µL	--	10-1 µL
Background	50 µL	--	--	30 µL	20 µL	--	--
Blank	50 µL	--	--	50 µL	--	--	--

Figure 14. Caspase-3 Activity Data. (Top) Readout for activity assay to validate active protein based on Caspase-3 Drug Discovery Kit by Enzo Life Sciences and the protocol provided in *"Expression, Purification, and Characterization of Caspases"* by Jean-Bernard Denault et Al. in Current Protocols in Protein Science (2002). Assay utilized fluorometric ligand Ac-DEVD-AMC. Excitation was measured at 380nm, emission was measured at 460nm with a cutoff at 435nm. **(Bottom)** Well compositions for 96-well assays.

Ni-NTA fractions were bag-dialyzed into 1L low salt Q-column buffer (25 mM Tris-HCL pH 8.0, 20 mM NaCl, 10 mM DTT, filtered at 0.2 um) for 2 hours and then another 1L for 24 hours. Pumps were primed on an AKTA HPLC for cation exchange chromatography using program Dual-Hi_Trap_Q_10mL_Equilibrate under Sprang > Sam (AKTA pure), the samples were loaded into the sample pump, and the program Dual-Hi_Trap_Q_10mL_Fast_Run_No_Pump_Wash_Sam was run. Protein eluted at ~25 mS/cm and was validated using SDS-PAGE (pg 63). The appropriate fractions were concentrated using a 10 MWCO concentrator, reducing the total volume down to 1 mL. This was then loaded into an FPLC with a G75 size exclusion column previously equilibrated with Size Exclusion Buffer (25 mM HEPEs pH 7.4, 50 mM NaCl, 1 mM EDTA, filtered at 0.2 um). The protein was eluted as a 120 kDa hetero-octamer using a flowrate of approximately 0.5 mL/min (pg 63)

Caspase-3 Positive Control Crystal

Caspase-3 was successfully crystallized (pg 66) using previously published methodologies for hanging drop cocrystal experiments with Caspase-3 and the known inhibitor Ac-DEVD-CHO. This crystal was generated in 100 mM sodium citrate, 5% glycerol, 10 mM DTT, 12-18% PEG 6k (Rotonda et al. 1997) and was shot at the APS in Chicago, IL by Dr. T.C. Mou. Indexing was done using *HKL2000*; further data assessment was done using *Phenix.Xtriage*; molecular replacement was done using
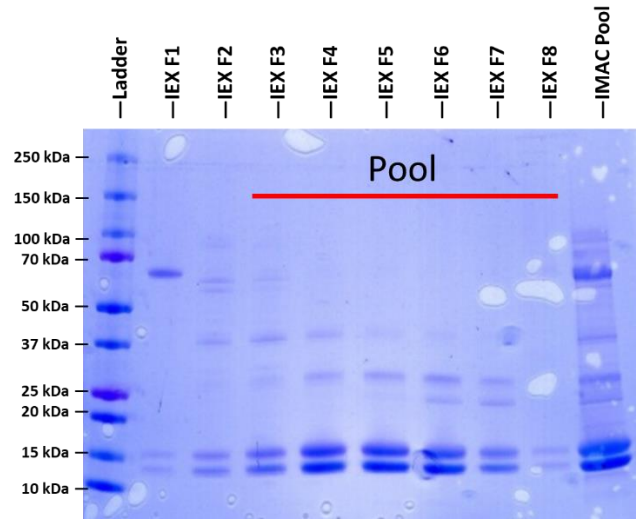
Figure 15. Caspase-3 Q-column SDS-PAGE. SDS-PAGE gels of caspase-3 after Q-column purification, with a Kaleidoscope Ladder (Lane 1) followed by Q-column fractions using an AKTA FPLC (lane 3-9) and the Ni-NTA fraction loaded into the Q-column (lane 10). Gel was stained using Coomassie Brilliant Blue.
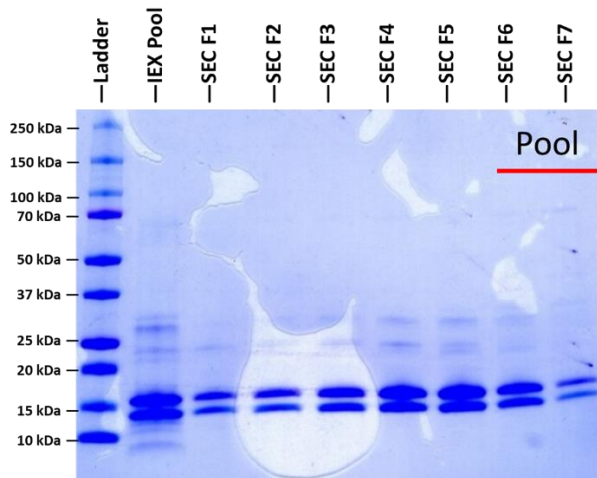

Figure 16. Caspase-3 Size Exclusion SDS-PAGE. SDS-PAGE gels of caspase-3 after S-column purification on a G75 column, with a Kaleidoscope Ladder (Lane 1) followed by a Q-column fraction using an AKTA FPLC (lane 2), followed by fractions purified on a G75 S-column (Lane 3-10). Gel was stained using Coomassie Brilliant Blue.

Phenix.phaser and PDB:1PAU as a reference model (Rotonda et. Al. 1997); and refinement

using was done using *Phenix.refine* along with visualization in *Coot* and *Pymol*. The final

structure (pg 67) was contained in space group $P2_12_12_1$, in a unit cell with parameters of a

= 69.81Å, b = 84.62Å, c = 96.79Å, α = 90º, β = 90º, γ = 90º. The structure showed good

completeness (93.8%) at the resolution shell for 1.74 Å, with 11270 to 12017 unique

reflections in that resolution shell (2.08 – 1.74 Å), as calculated with *Phenix.Xtriage*. This

is on par with other published caspase-ligand structures utilizing reversible inhibitors based

on endogenous substrates (Rotonda et al. 1997, PDB: 1PAU; Fang et al 2006, PDB: 2H5I).

Caspase-3 Cocrystals with Natural Products

Based on the previous success of crystal generation with a positive control, further

crystallographic trials were conducted with natural product inhibitors previously identified

by the Stierle Lab. To this end, several 96-well sitting drop experiments were conducted

with traditional 96-well crystal screens: JSGC I – IV (Lesley and Wilson 2005), PEG1-2

(Qiagen), and 24-well hanging drop experiments with custom conditions (Plate 1: 0.1 M

Sodium Citrate with 1.6 to 2.2 Ammonium Sulfate along the Y-axis, and pH 2.4 to 4.9

along the X-axis; Plate 2: 0.1M Tris-HCl, 0.2M Ammonium Sulfate, 30-45% 2-methyl-

2,4-pentandiol along the Y-axis, pH 7 to 6 along the X-axis) at both 4ºC and 25ºC. Ligands

were prepared in DMSO at 6 mg/mL and mixed with caspase-3 at a ratio 20x the recorded

IC_{50} (Mittl et al. 1997). Crystal plates were stored at 4 and 25ºC, screened using visible

light microscopy to identify crystals and UV-microscopy to verify the crystals contain

protein (Desbois et al 2013).

Conclusions and Future Directions

For the positive control experiment, we were able to successfully generate crystals of caspase-3 with Ac-DEVD-CHO at 1.75 Å (pg 66, 67) with a high level of completeness (93.8%). Concerning the cocrystal experiments with natural product inhibitors, microcrystals were generated for DNA 66 (pg 69, 70; Newman, Cragg, and Stierle et al. 2017) and DNA 82 (unpublished) under the conditions in JCSG3 wells H9 and H10 (H9: 0.1 M Citric acid pH 3.5, 1.6 M Ammonium Sulfate, final pH 4.0; H10: 2.0 M Sodium Chloride, 10% (w/v) PEG 6,000 respectively). Unfortunately, larger crystals could not be generated for diffraction studies, which were required for handling and transport. Microcrystals can be incredibly hard to isolate and unstable during transport to a beamline.

While this project was more successful than the caspase-1 project, we were still unable to produce publishable results. The cocrystallization of caspase-3 with a small molecule inhibitor can be further explored by using the microcrystals generated as seeds for further crystallization studies. By moving the crystals to new solutions with high protein concentration, growing them to a diffractable size might be possible.
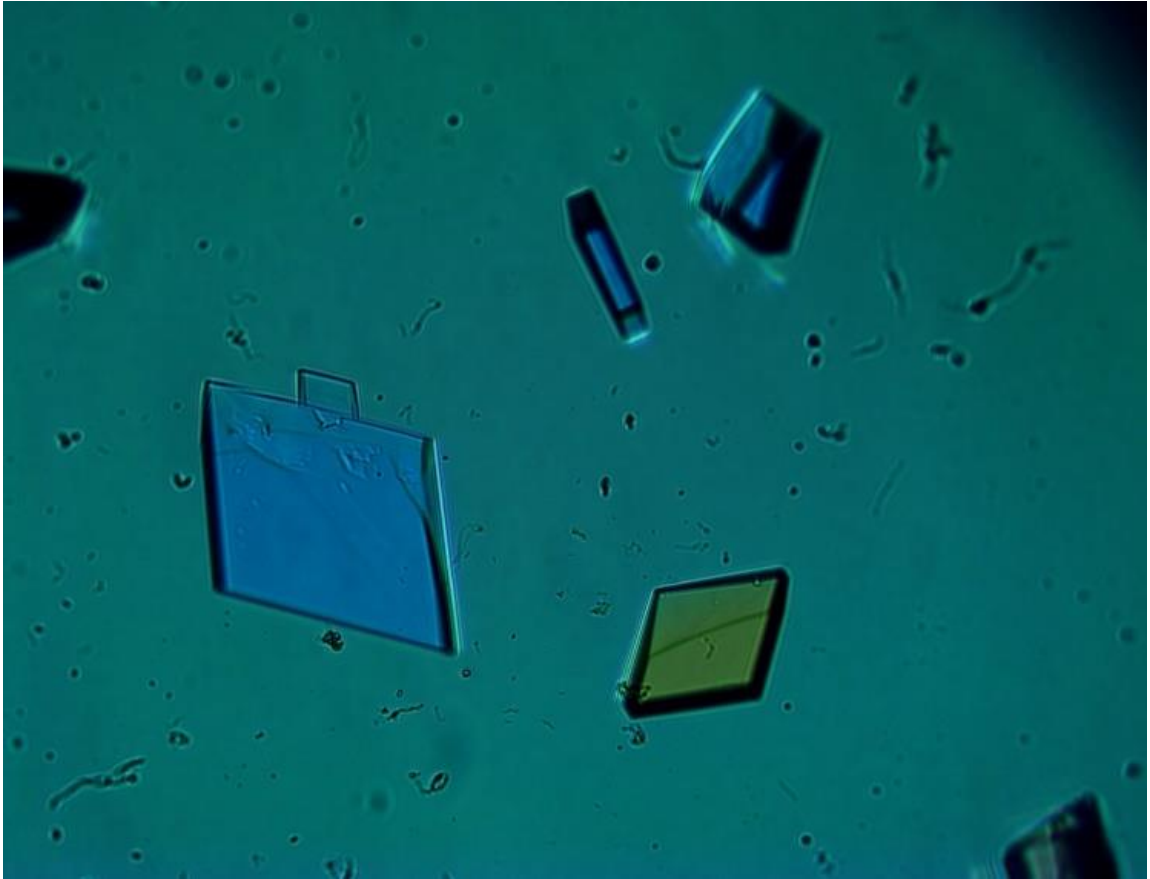
Figure 17. Caspase-3 and Ac-DEVD-CHO Crystals. Protein crystals of caspase-3

bound to Ac-DEVD-CHO generated in 100 mM Na-citrate, 5% glycerol, 10 mM DTT,

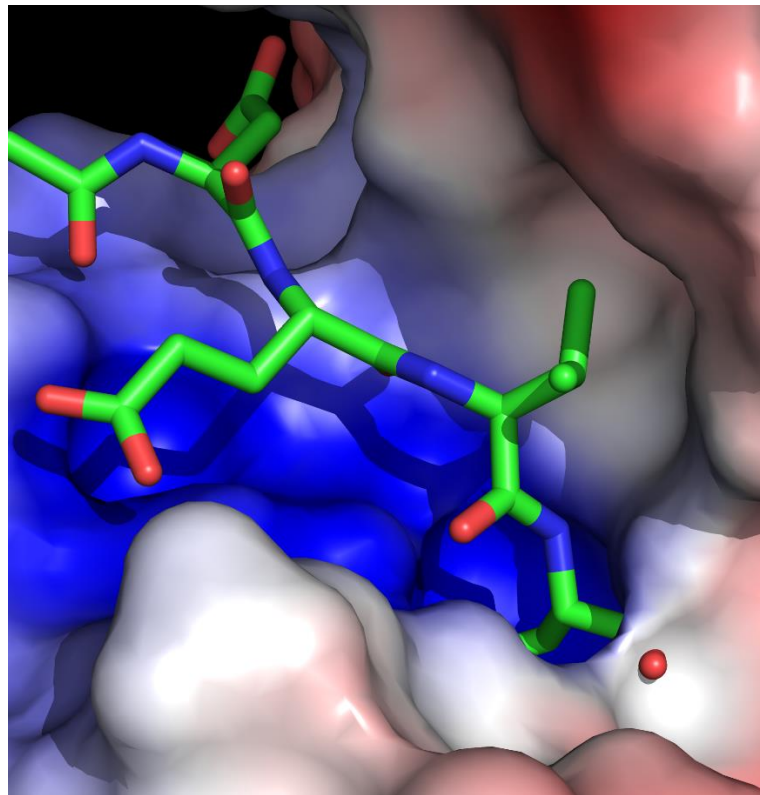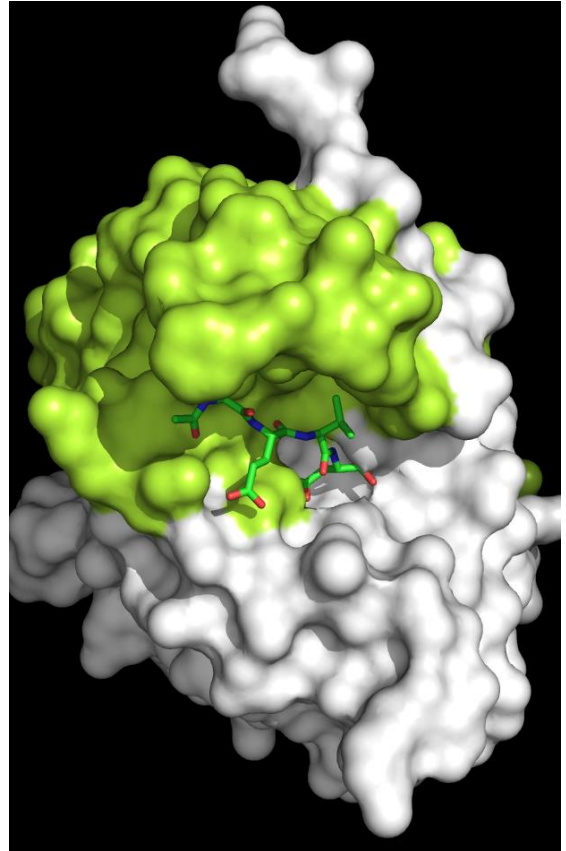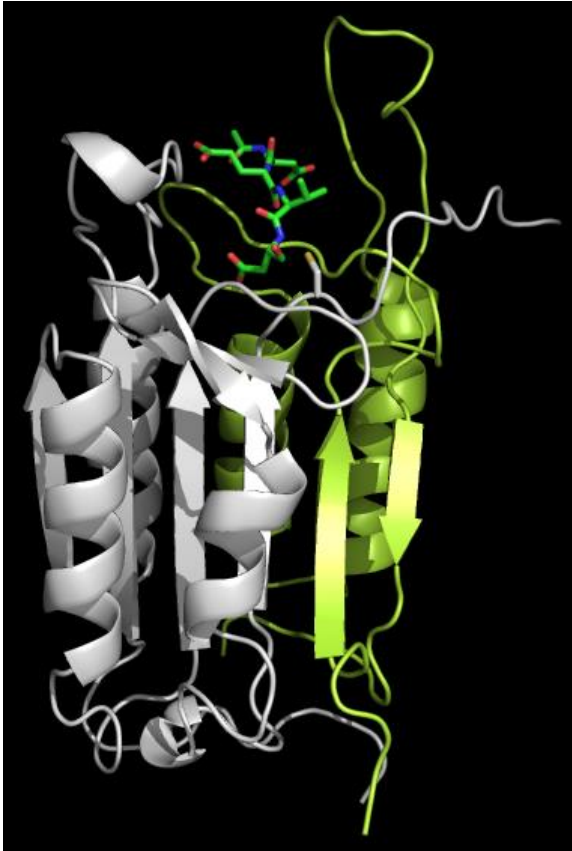12-18% PEG 6k. Crystals diffracted at 1.74 A with 93% completeness.

Figure 18. Caspase-3 Crystal Screen Captures. (Left) Image capture of caspase-3 positive control from the side. Green ribbon depicts the caspase-3 small subunit and the gray ribbon shows the large subunit. Green stick model represents Ac-DEVD-CHO, gray stick model represents cystine 285, the active residue which is responsible for proteolytic attack. **(Right)** Surface representation of caspase-3's binding site viewed from the top down**.** (**Bottom**) A closer zoom on the electrostatic potential map for the caspase-3 binding site with Ac-DEVD-CHO bound. This further illustrates the S1 to S4 sites (lower right to upper left) represented in loops 1-4 (foreground). Images were collected using Pymol software.
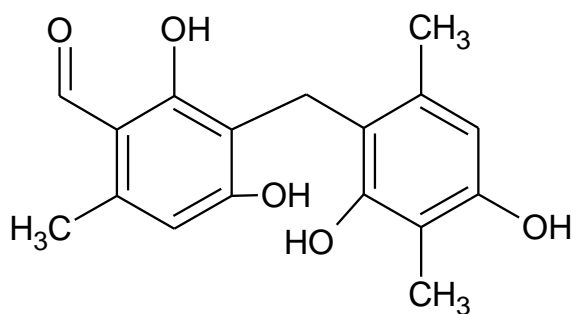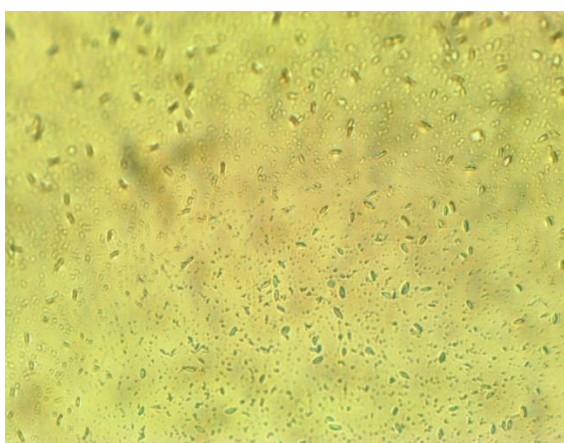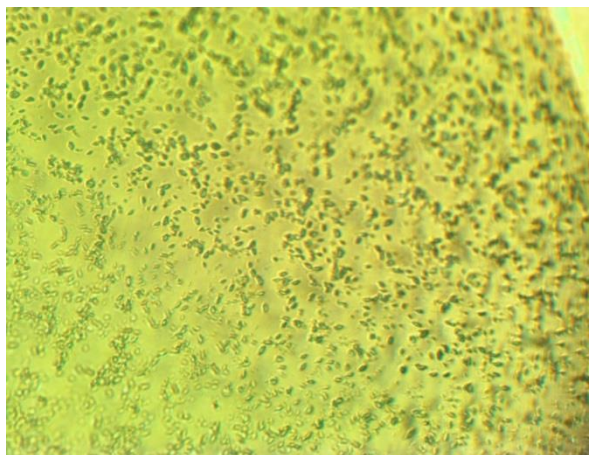
Figure 19. Caspase-3 and DNA 82 Microcrystals. Human caspase-3 sitting drop cocrystal experiments with natural product inhibitor DNA 82. **(Top)** Image depicts microcrystals from JCSG 3 well H9. **(Middle)** Image depicts microcrystals from JCSG 3 well H10. Images were taken using light microscope in the Crystallography Core at University of Montana. **(Bottom)** Natural product inhibitor DNA 82.

Figure 20. Caspase-3 and DNA 66 Microcrystals. Human caspase-3 sitting drop cocrystal experiments with natural product inhibitor DNA 66. **(Top)** Image depicts microcrystals from JCSG 3 well H9. **(Middle)** Image depicts microcrystals from JCSG 3 well H10. Images were taken using light microscope in the Crystallography Core at University of Montana. **(Bottom)** Natural product inhibitor DNA 66.
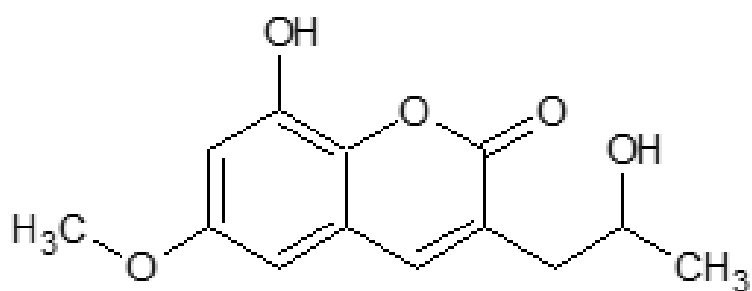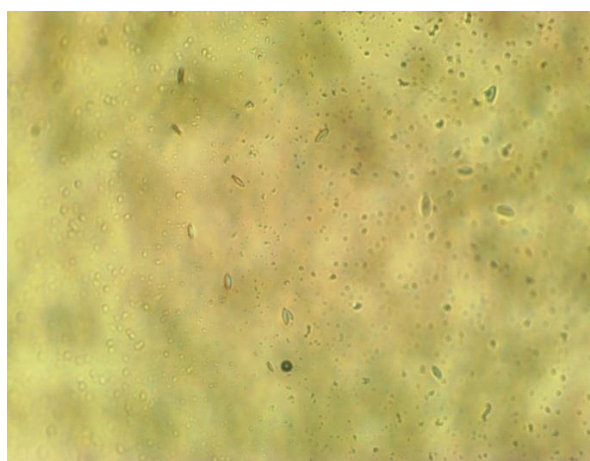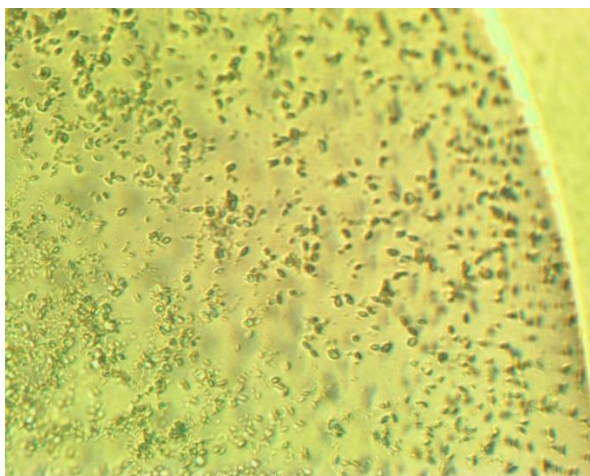
This does not solve the issue of peptide stabilization, which I believe is a 2-fold problem (ligand length and protein dynamics) but exemplified by one process (dynamics). The action of the caspases is highly dynamic (Fang et al. 2006); there is a substantial amount of domain translocation during substrate binding, lysis, and release, particularly around the ligand-binding cleft and the S4-S3 sites. This means that stabilizing the peptide complex, which is essential to high resolution protein crystals, can be extremely difficult and requires a host of interactions at spatially distinct sites (S1 to S4, not just S1). While this can be accomplished with simple, extended peptide chains, it is not a trivial task for non-peptide-based inhibitors. To this end, I think crystallization would have a higher probability for success utilizing inhibitors with either a higher affinity or with more extended structure. These might be capable of stabilizing more spatially distinct sites in the caspase-3 binding cleft, similar to that of peptide-based caspase inhibitors. A similar approach was employed when developing the NS3 protease inhibitor, Boceprevir (Howe et al 2013).

References

Ajikumar, P. K., Xiao, W. H., Tyo, K. E., Wang, Y., Simeon, F., Leonard, E., Stephanopoulos, G., et al. (2010). Isoprenoid pathway optimization for Taxol precursor overproduction in Escherichia coli. Science, 330(6000), 70-74. DOI: 10.1126/science.1191652

Arenz, S., Ramu, H., Gupta, P., Berninghausen, O., Beckmann, R., Vázquez-Laslop, N., et al. (2014). Molecular basis for erythromycin-dependent ribosome stalling during translation of the ErmBL leader peptide. Nature communications, 5, 3501.

Bernardini, S., Tiezzi, A., Laghezza Masci, V., & Ovidi, E. (2018). Natural products for human health: an historical overview of the drug discovery approaches. Natural product research, 32(16), 1926-1950. DOI: https://doi.org/10.1080/14786419.2017.1356838

Biggs, B. W., De Paepe, B., Santos, C. N. S., De Mey, M., & Ajikumar, P. K. (2014). Multivariate modular metabolic engineering for pathway and strain optimization. Current opinion in biotechnology, 29, 156-162. DOI: https://doi.org/10.1016/j.copbio.2014.05.005

Biggs, B. W., Rouck, J. E., Kambalyal, A., Arnold, W., Lim, C. G., De Mey, M., Ajikumar, P. K. et al. (2016). Orthogonal assays clarify the oxidative biochemistry of Taxol P450 CYP725A4. ACS chemical biology, 11(5), 1445-1451. DOI: 10.1021/acschembio.5b00968

Blin, K., Kim, H. U., Medema, M. H., & Weber, T. (2017). Recent development of antiSMASH and other computational approaches to mine secondary metabolite biosynthetic gene clusters. Briefings in bioinformatics. DOI: https://doi.org/10.1093/bib/bbx146

Bocioaga, D., & Mitman, G. G. (2003). 10 Chlamydomonas acidophila from the berkeley pit lake–a strain adapted to an extreme environment. Journal of Phycology, 39, 4-4. DOI: https://doi.org/10.1111/j.0022-3646.2003.03906001_10.x

Bok, J. W., & Keller, N. P. (2004). LaeA, a regulator of secondary metabolism in Aspergillus spp. Eukaryotic cell, 3(2), 527-535. DOI: 10.1128/EC.3.2.527-535.2004

Bragg, W. H., & Bragg, W. L. (1913). The reflection of X-rays by crystals. Proc. R. Soc. Lond. A, 88(605), 428-438.

Campbell, W. (2012). History of avermectin and ivermectin, with notes on the history of other macrocyclic lactone antiparasitic agents. Current pharmaceutical biotechnology, 13(6), 853-865. DOI: https://doi.org/10.2174/138920112800399095

Carrillo, A., Stewart, K. D., Sham, H. L., Norbeck, D. W., Kohlbrenner, W. E., Leonard, J. M., ... & Molla, A. (1998). In vitro selection and characterization of human immunodeficiency virus type 1 variants with increased resistance to ABT-378, a novel protease inhibitor. Journal of virology, 72(9), 7532-7541. DOI: 0022-538X/98/$04.0010

Chen, Y., Garcia de Lomana, M., Friedrich, N. O., & Kirchmair, J. (2018). Characterization of the chemical space of known and readily obtainable natural products. Journal of chemical information and modeling, 58(8), 1518-1532. DOI: 10.1021/acs.jcim.8b00302

Cragg, G. M., Grothaus, P. G., & Newman, D. J. (2009). Impact of natural products on developing new anti-cancer agents. Chemical reviews, 109(7), 3012-3043. DOI: 10.1021/cr900019j

Cuzick, J., Otto, F., Baron, J. A., Brown, P. H., Burn, J., Greenwald, P., ... & Thun, M. (2009). Aspirin and non-steroidal anti-inflammatory drugs for cancer prevention: an international consensus statement. The lancet oncology, 10(5), 501-507. DOI: https://doi.org/10.1016/S1470-2045(09)70035-X

Da Rocha, A. B., Lopes, R. M., & Schwartsmann, G. (2001). Natural products in anticancer therapy. Current opinion in pharmacology, 1(4), 364-369. DOI: https://doi.org/10.1016/S1471-4892(01)00063-7

de Jong, A., Pietersma, H., Cordes, M., Kuipers, O. P., & Kok, J. (2012). PePPER: a webserver for prediction of prokaryote promoter elements and regulons. BMC genomics, 13(1), 299. DOI: https://doi.org/10.1186/1471-2164-13-299

Denault, J. B., & Salvesen, G. S. (2002). Caspases: keys in the ignition of cell death. Chemical reviews, 102(12), 4489-4500. DOI: 10.1021/cr010183n

Desbois, S., Seabrook, S. A., & Newman, J. (2013). Some practical guidelines for UV imaging in the protein crystallization laboratory. Acta Crystallographica Section F: Structural Biology and Crystallization Communications, 69(2), 201-208. DOI: https://doi.org/10.1107/S1744309112048634

Dias, D. A., Urban, S., & Roessner, U. (2012). A historical overview of natural products in drug discovery. Metabolites, 2(2), 303-336. DOI: https://doi.org/10.3390/metabo2020303

Edwards, A. L., Matsui, T., Weiss, T. M., & Khosla, C. (2014). Architectures of whole-module and bimodular proteins from the 6-deoxyerythronolide B synthase. Journal of molecular biology, 426(11), 2229-2245. DOI: https://doi.org/10.1016/j.jmb.2014.03.015

Esnouf, R., Ren, J., Ross, C., Jones, Y., Stammers, D., & Stuart, D. (1995). Mechanism of inhibition of HIV-1 reverse transcriptase by non-nucleoside inhibitors. Nature Structural and Molecular Biology, 2(4), 303. DOI: https://doi.org/10.1038/nsb0495-303

Fan, W., Dai, Y., Xu, H., Zhu, X., Cai, P., Wang, L., et al. (2014). Caspase-3 Modulates Regenerative Response After Stroke. Stem cells, 32(2), 473-486. DOI: https://doi.org/10.1002/stem.1503

Fang, B., Boross, P. I., Tozser, J., & Weber, I. T. (2006). Structural and kinetic analysis of caspase-3 reveals role for s5 binding site in substrate recognition. Journal of molecular biology, 360(3), 654-666. DOI: https://doi.org/10.1016/j.jmb.2006.05.041

Faurant, C. (2011). From bark to weed: The history of artemisinin. Parasite: journal de la Société Française de Parasitologie, 18(3), 215. doi: 10.1051/parasite/2011183215

Garcia-Calvo, M., Peterson, E. P., Rasper, D. M., Vaillancourt, J. P., Zamboni, R., Nicholson, D. W., & Thornberry, N. A. (1999). Purification and catalytic properties of human caspase family members. Cell death and differentiation, 6(4), 362. DOI: https://doi.org/10.1038/sj.cdd.4400497

Gardiner, D. M., Waring, P., & Howlett, B. J. (2005). The epipolythiodioxopiperazine (ETP) class of fungal toxins: distribution, mode of action, functions and biosynthesis. Microbiology, 151(4), 1021-1032. DOI: 10.1099/mic.0.27847-0

Ghorbani-Nasrabadi, R., Greiner, R., Alikhani, H. A., Hamedi, J., & Yakhchali, B. (2013). Distribution of actinomycetes in different soil ecosystems and effect of media composition on extracellular phosphatase activity. Journal of soil science and plant nutrition, 13(1), 223-236. DOI: http://dx.doi.org/10.4067/S0718-95162013005000020

Ghosh, A. K., Dawson, Z. L., & Mitsuya, H. (2007). Darunavir, a conceptually new HIV-1 protease inhibitor for the treatment of drug-resistant HIV. Bioorganic & medicinal chemistry, 15(24), 7576-7580. DOI: https://doi.org/10.1016/j.bmc.2007.09.010

Ghosh, A. K., Yu, X., Osswald, H. L., Agniswamy, J., Wang, Y. F., Amano, M., et al. (2015). Structure-Based Design of Potent HIV-1 Protease Inhibitors with Modified P1-Biphenyl Ligands: Synthesis, Biological Evaluation, and Enzyme–Inhibitor X-ray Structural Studies. Journal of medicinal chemistry, 58(13), 5334-5343. DOI: 10.1021/acs.jmedchem.5b00676

Griffith, R. S. (1981). Introduction to vancomycin. Reviews of infectious diseases, 3(Supplement), S200-S204. DOI: 0162-0886/81/0306-0002$02.00

Guzik, K., Zak, K. M., Grudnik, P., Magiera, K., Musielak, B., Törner, R., et al. (2017). Small-molecule inhibitors of the Programmed Cell Death-1/Programmed Death-Ligand 1 (PD-1/PD-L1) interaction via transiently induced protein states and dimerization of PD-L1. Journal of medicinal chemistry, 60(13), 5857-5867. DOI: 10.1021/acs.jmedchem.7b00293

Hong, E. J., Kim, N. K., Lee, D., Kim, W. G., & Lee, I. (2015). Overexpression of the laeA gene leads to increased production of cyclopiazonic acid in Aspergillus fumisynnematus. Fungal biology, 119(11), 973-983. DOI: https://doi.org/10.1016/j.funbio.2015.06.006

Hook, G., Jacobsen, J. S., Grabstein, K., Kindy, M., & Hook, V. (2015). Cathepsin B is a new drug target for traumatic brain injury therapeutics: evidence for E64d as a promising lead drug candidate. Frontiers in neurology, 6, 178. DOI: https://doi.org/10.3389/fneur.2015.00178

Jakubiec-Krzesniak, K., Rajnisz-Mateusiak, A., Guspiel, A., Ziemska, J., & Solecka, J., (2018). Secondary Metabolites of Actinomycetes and their Antibacterial, Antifungal and Antiviral Properties. Polish journal of microbiology, 67(3), 259-272. DOI: https://doi.org/10.21307/pjm-2018-048

Kendrew, J. C., Bodo, G., Dintzis, H. M., Parrish, R. G., Wyckoff, H., & Phillips, D. C. (1958). A three-dimensional model of the myoglobin molecule obtained by x-ray analysis. Nature, 181(4610), 662-666. DOI: https://doi.org/10.1038/181662a0

Khaldi, N., Seifuddin, F. T., Turner, G., Haft, D., Nierman, W. C., Wolfe, K. H., & Fedorova, N. D. (2010). SMURF: genomic mapping of fungal secondary metabolite clusters. Fungal Genetics and Biology, 47(9), 736-741. DOI: https://doi.org/10.1016/j.fgb.2010.06.003

Khalil, Z. G., Cruz-Morales, P., Licona-Cassani, C., Marcellin, E., & Capon, R. J. (2018). Inter-Kingdom beach warfare: Microbial chemical communication activates natural chemical defences. The ISME journal, 1. DOI: https://doi.org/10.1038/s41396-018-0265-z

Khalil, Z. G., Kalansuriya, P., & Capon, R. J. (2014). Lipopolysaccharide (LPS) stimulation of fungal secondary metabolism. Mycology, 5(3), 168. DOI: 10.1080/21501203.2014.930530

Kinghorn, A. D., Chin, Y. W., & Swanson, S. M. (2009). Discovery of natural product anticancer agents from biodiverse organisms. Current opinion in drug discovery & development, 12(2), 189.

Leelananda, S. P., & Lindert, S. (2016). Computational methods in drug discovery. Beilstein journal of organic chemistry, 12(1), 2694-2718. DOI: 10.3762/bjoc.12.267

Li, J. W. H., & Vederas, J. C. (2009). Drug discovery and natural products: end of an era or an endless frontier?. Science, 325(5937), 161-165. DOI: 10.1126/science.1168243

Li, X. F., Lu, Z. H., Zhao, G. L., Wu, H., & Yu, Y. G. (2012). A facile whole-cell biocatalytic approach to regioselective synthesis of monoacylated 1-β-d-arabinofuranosylcytosine: Influence of organic solvents. Bioresource technology, 114, 6-11. DOI: https://doi.org/10.1016/j.biortech.2012.03.056

Ling, L. L., Schneider, T., Peoples, A. J., Spoering, A. L., Engels, I., Conlon, B. P., et al. (2015). A new antibiotic kills pathogens without detectable resistance. Nature, 517(7535), 455. DOI: https://doi.org/10.1038/nature14098

MacKenzie, S. H., Schipper, J. L., & Clark, A. C. (2010). The potential for caspases in drug discovery. Current opinion in drug discovery & development, 13(5), 568.

Manabat, C., Han, B. H., Wendland, M., Derugin, N., Fox, C. K., Choi, J., et al. (2003). Reperfusion differentially induces caspase-3 activation in ischemic core and penumbra after stroke in immature brain. Stroke, 34(1), 207-213.

Maravic, G. (2004). Macrolide resistance based on the Erm-mediated rRNA methylation. Current Drug Targets-Infectious Disorders, 4(3), 193-202. DOI: https://doi.org/10.2174/1568005043340777

Martín, J., García-Estrada, C., Rumbero, Á., Recio, E., Albillos, S. M., Ullán, R. V., & Martín, J. F. (2011). Characterization of an autoinducer of penicillin biosynthesis in Penicillium chrysogenum. Applied and environmental microbiology, AEM-00059. DOI: 10.1128/AEM.00059-11

Mazid, M., Khan, T. A., & Mohammad, F. (2011). Role of secondary metabolites in defense mechanisms of plants. Biology and medicine, 3(2), 232-249.

Mckenzie, B., Reinke, S., Branton, W., Lu, J. Q., & Power, C. (2014). Activation of multiple inflammasomes within the central nervous system during experimental autoimmune encephalomyelitis and multiple sclerosis. Journal of Neuroimmunology, 275(1), 163. DOI: https://doi.org/10.1016/j.jneuroim.2014.08.438

Medema, M. H., Blin, K., Cimermancic, P., de Jager, V., Zakrzewski, P., Fischbach, M. A., et al. (2011). antiSMASH: rapid identification, annotation and analysis of secondary metabolite biosynthesis gene clusters in bacterial and fungal genome sequences. Nucleic acids research, 39(suppl_2), W339-W346. DOI: https://doi.org/10.1093/nar/gkr466
Yang, S. (1998). The divine farmer's materia medica: a translation of the Shen Nong Ben Cao Jing. Blue Poppy Enterprises, Inc.

Melvin, J. Y. (2012). Simulating the drug discovery pipeline: a Monte Carlo approach. Journal of Cheminformatics, 4(1), 32. DOI: https://doi.org/10.1186/1758-2946-4-32

Mendes, V., & Blundell, T. L. (2017). Targeting tuberculosis using structure-guided fragment-based drug design. Drug discovery today, 22(3), 546-554. DOI: https://doi.org/10.1016/j.drudis.2016.10.003

Michel, K. H., Chaney, M. O., Jones, N. D., Hoehn, M. M., & Nagarajan, R. (1974). Epipolythiopiperazinedione antibiotics from Penicillium turbatum. The Journal of antibiotics, 27(1), 57-64. DOI: https://doi.org/10.7164/antibiotics.27.57

Michel, K. H., Demarco, P. V., & Nagarajan, R. (1977). The isolation and structure elucidation of macrocyclic lactone antibiotic, A26771B. The Journal of antibiotics, 30(7), 571-575. DOI: https://doi.org/10.7164/antibiotics.30.571

Mittl, P. R., Di Marco, S., Krebs, J. F., Bai, X., Karanewsky, D. S., Priestle, J. P., et al. (1997). Structure of recombinant human CPP32 in complex with the tetrapeptide acetyl-Asp-Val-Ala-Asp fluoromethyl ketone. Journal of Biological Chemistry, 272(10), 6539-6547. DOI: 10.1074/jbc.272.10.6539

Moloney, M. F. (1919). Irish ethno-botany and the evolution of medicine in Ireland. MH Gill.

Newman, Cragg, Stierle, Stierle, et al. "Novel Metabolites from Extremophilic Microbes Isolated from Toxic Waste Sites." Chemical Biology of Natural Products, vol. 1, 2017, pp 371-372.

Newman, D. J., & Cragg, G. M. (2012). Natural products as sources of new drugs over the 30 years from 1981 to 2010. Journal of natural products, 75(3), 311-335. DOI: 10.1021/np200906s

Nichols, D., Cahoon, N., Trakhtenberg, E. M., Pham, L., Mehta, A., Belanger, A., Kanigan T., Lewis K., Epstein, S. S. (2010). Use of ichip for high-throughput in situ cultivation of "uncultivable" microbial species. Applied and environmental microbiology, 76(8), 2445-2450. DOI: 10.1128/AEM.01754-09

Nickerson, K. W., Atkin, A. L., & Hornby, J. M. (2006). Quorum sensing in dimorphic fungi: farnesol and beyond. Applied and environmental microbiology, 72(6), 3805-3813. DOI: 10.1128/AEM.02765-05

Oh, D. C., Kauffman, C. A., Jensen, P. R., & Fenical, W. (2007). Induced production of emericellamides A and B from the marine-derived fungus Emericella sp. in competing co-culture. Journal of natural products, 70(4), 515-520. DOI: 10.1021/np060381f

Okano, A., Isley, N. A., & Boger, D. L. (2017). Peripheral modifications of [Ψ [CH2NH] Tpg4] vancomycin with added synergistic mechanisms of action provide durable and potent antibiotics. Proceedings of the National Academy of Sciences, 201704125. DOI: https://doi.org/10.1073/pnas.1704125114

Onaka, H. (2017). Novel antibiotic screening methods to awaken silent or cryptic secondary metabolic pathways in actinomycetes. The Journal of antibiotics, 70(8), 865. DOI: https://doi.org/10.1038/ja.2017.51

Osbourn, A. E., & Field, B. (2009). Operons. *Cellular and Molecular Life Sciences*, *66*(23), 3755-3775. DOI: 10.1007/s00018-009-0114-3

Performance Standards for Antimicrobial Disk and Dilution Susceptibility Tests for Bacteria Isolated From Animals, 5th Edition

Qinghaosu Antimalaria Coordinating Research Group. (1979). Antimalaria studies on qinghaosu. Chinese medical journal, 92(12), 811-816.

Rano, T. A., Timkey, T., Peterson, E. P., Rotonda, J., Nicholson, D. W., Becker, J. W., Thornberry, N. A., et al. (1997). A combinatorial approach for determining protease specificities: application to interleukin-1β converting enzyme (ICE). Chemistry & biology, 4(2), 149-155. DOI: https://doi.org/10.1016/S1074-5521(97)90258-1

Roberts, N. A., Martin, J. A., Kinchington, D., Broadhurst, A. V., Craig, J. C., Duncan, I. B., et al. (1990). Rational design of peptide-based HIV proteinase inhibitors. Science, 248(4953), 358-361.Romanowski et al. "An allosteric circuit in caspase-1." Journal of molecular biology vol 381, no. 5 (2008): 1157-1167. DOI: 10.1126/science.2183354

Roschitzki-Voser, H., Schroeder, T., Lenherr, E. D., Frölich, F., Schweizer, A., Donepudi, M., Grütter, G., et al. (2012). Human caspases in vitro: expression, purification and kinetic characterization. Protein expression and purification, 84(2), 236-246. DOI: https://doi.org/10.1016/j.pep.2012.05.009

Rotonda, J., Nicholson, D. W., Fazil, K. M., Gallant, M., Gareau, Y., Labelle, M., Thornberry, N., et al. (1996). The three-dimensional structure of apopain/CPP32, a key mediator of apoptosis. Nature Structural and Molecular Biology, 3(7), 619. DOI: https://doi.org/10.1038/nsb0796-619

Roze, L. V., Chanda, A., Wee, J., Awad, D., & Linz, J. E. (2011). Stress-related transcription factor atfB integrates secondary metabolism with the oxidative stress response in Aspergilli. Journal of Biological Chemistry, jbc-M111. DOI: 10.1074/jbc.M111.253468

Rutledge, P. J., & Challis, G. L. (2015). Discovery of microbial natural products by activation of silent biosynthetic gene clusters. Nature reviews microbiology, 13(8), 509. DOI: https://doi.org/10.1038/nrmicro3496

Santajit, S., & Indrawattana, N. (2016). Mechanisms of antimicrobial resistance in ESKAPE pathogens. BioMed research international, 2016.

Sarikaya-Bayram, Ö., Palmer, J. M., Keller, N., Braus, G. H., & Bayram, Ö. (2015). One Juliet and four Romeos: VeA and its methyltransferases. Frontiers in microbiology, 6, 1.

Schäfer, M., Schneider, T. R., & Sheldrick, G. M. (1996). Crystal structure of vancomycin. Structure, 4(12), 1509-1515. DOI: https://doi.org/10.1016/S0969-2126(96)00156-6

Schatz, A., Bugle, E., & Waksman, S. A. (1944). Streptomycin, a Substance Exhibiting Antibiotic Activity Against Gram-Positive and Gram-Negative Bacteria.∗. Proceedings of the Society for Experimental Biology and Medicine, 55(1), 66-69. DOI: https://doi.org/10.3181/00379727-55-14461

Schmidt, J., Khalil, Z., Capon, R. J., & Stark, C. B. (2014). Heronapyrrole D: A case of co-inspiration of natural product biosynthesis, total synthesis and biodiscovery. Beilstein journal of organic chemistry, 10, 1228. DOI: 10.3762/bjoc.10.121

Semighini, C. P., Hornby, J. M., Dumitru, R., Nickerson, K. W., & Harris, S. D. (2006). Farnesol-induced apoptosis in Aspergillus nidulans reveals a possible mechanism for antagonistic interactions between fungi. Molecular microbiology, 59(3), 753-764. DOI: https://doi.org/10.1111/j.1365-2958.2005.04976.x

Shi, L., Wang, X., Wang, J., Zhang, P., Qi, F., Cai, M., ... & Zhou, X. (2018). Transcriptome analysis of Δmig1Δmig2 mutant reveals their roles in methanol catabolism, peroxisome biogenesis and autophagy in methylotrophic yeast Pichia pastoris. Genes & genomics, 1-14. DOI: https://doi.org/10.1007/s13258-017-0641-5

Smith, S., & Tsai, S. C. (2007). The type I fatty acid and polyketide synthases: a tale of two megasynthases. Natural product reports, 24(5), 1041-1072. DOI: 10.1039/B603600G

Stierle, A. A., Stierle, D. B., & Kelly, K. (2006). Berkelic acid, a novel spiroketal with selective anticancer activity from an acid mine waste fungal extremophile. The Journal of organic chemistry, 71(14), 5357-5360. DOI: 10.1021/jo060018d

Stierle, A. A., Stierle, D. B., & Patacini, B. (2008). The berkeleyamides, amides from the acid lake fungus Penicillum rubrum. Journal of natural products, 71(5), 856-860. DOI: 10.1021/np0705054

Stierle, A. A., Stierle, D. B., Decato, D., Priestley, N. D., Alverson, J. B., Hoody, J., McGrath, k., et al. (2017). The berkeleylactones, antibiotic macrolides from fungal coculture. Journal of natural products, 80(4), 1150-1160. DOI: 10.1021/acs.jnatprod.7b00133

Stierle, A. A., Stierle, D. B., Mitman, G. G., Snyder, S., Antczak, C., & Djaballah, H. (2014). Phomopsolides and related compounds from the alga-associated fungus, Penicillium clavigerum. Natural product communications, 9(1), 87-90.

Stierle, D. B., Stierle, A. A., & Patacini, B. (2007). The berkeleyacetals, three meroterpenes from a deep water acid mine waste Penicillium. Journal of natural products, 70(11), 1820-1823. DOI: 10.1021/np070329z

Strieker, M., Tanović, A., & Marahiel, M. A. (2010). Nonribosomal peptide synthetases: structures and dynamics. Current opinion in structural biology, 20(2), 234-240. DOI: https://doi.org/10.1016/j.sbi.2010.01.009

Su, J. H., Zhao, M., Anderson, A. J., Srinivasan, A., & Cotman, C. W. (2001). Activated caspase-3 expression in Alzheimer's and aged control brain: correlation with Alzheimer pathology. Brain research, 898(2), 350-357. DOI: https://doi.org/10.1016/S0006-8993(01)02018-2

Su, X. Z., & Miller, L. H. (2015). The discovery of artemisinin and the Nobel Prize in Physiology or Medicine. Science China Life Sciences, 58(11), 1175-1179. DOI: https://doi.org/10.1007/s11427-015-4948-7

Suguna, K. A., Padlan, E. A., Smith, C. W., Carlson, W. D., & Davies, D. R. (1987). Binding of a reduced peptide inhibitor to the aspartic proteinase from Rhizopus chinensis: implications for a mechanism of action. Proceedings of the National Academy of Sciences, 84(20), 7009-7013. DOI: https://doi.org/10.1073/pnas.84.20.7009

Suzuki, Y., Tsunoda, T., Sese, J., Taira, H., Mizushima-Sugano, J., Hata, H., et al. (2001). Identification and characterization of the potential promoter regions of 1031 kinds of human genes. Genome research, 11(5), 677-684. DOI: 10.1101/gr.164001

Thornberry, N. A., Rano, T. A., Peterson, E. P., Rasper, D. M., Timkey, T., Garcia-Calvo, M., et al.1997). A combinatorial approach defines specificities of members of the caspase family and granzyme B Functional relationships established for key mediators of apoptosis. Journal of Biological Chemistry, 272(29), 17907-17911. DOI: 10.1074/jbc.272.29.17907

Van Montfort, R. L., & Workman, P. (2017). Structure-based drug design: aiming for a perfect fit. Essays in biochemistry, 61(5), 431-437. DOI: 10.1042/EBC20170052

Vander-Molen, K. M., Raja, H. A., El-Elimat, T., & Oberlies, N. H. (2013). Evaluation of culture media for the production of secondary metabolites in a natural products screening program. Amb Express, 3(1), 71. DOI: https://doi.org/10.1186/2191-0855-3-71

Vila-Farres, X., Chu, J., Inoyama, D., Ternei, M. A., Lemetre, C., Cohen, L. J., et al. (2017). Antimicrobials inspired by nonribosomal peptide synthetase gene clusters. Journal of the American Chemical Society, 139(4), 1404-1407. DOI: 10.1021/jacs.6b11861

Vogl, T., Sturmberger, L., Fauland, P. C., Hyden, P., Fischer, J. E., Schmid, C., et al. (2018). Methanol independent induction in Pichia pastoris by simple derepressed overexpression of single transcription factors. Biotechnology and bioengineering, 115(4), 1037-1050. DOI: https://doi.org/10.1002/bit.26529

Wagner, D. C., Riegelsberger, U. M., Michalk, S., Härtig, W., Kranz, A., & Boltze, J. (2011). Cleaved caspase-3 expression after experimental stroke exhibits different phenotypes and is predominantly non-apoptotic. Brain research, 1381, 237-242. DOI: https://doi.org/10.1016/j.brainres.2011.01.041

Wakefield, J., Hassan, H. M., Jaspars, M., Ebel, R., & Rateb, M. E. (2017). Dual induction of new microbial secondary metabolites by fungal bacterial co-cultivation. Frontiers in microbiology, 8, 1284. DOI: https://doi.org/10.3389/fmicb.2017.01284

Wang, X., Wang, Q., Wang, J., Bai, P., Shi, L., Shen, W., et al. (2016). Mit1 transcription factor mediates methanol signaling and regulates alcohol oxidase 1 promoter in Pichia pastoris. Journal of Biological Chemistry, jbc-M115. DOI: 10.1074/jbc.M115.692053

Whitty, A. (2011). Growing PAINS in academic drug discovery. Future medicinal chemistry, 3(7), 797-801. DOI: https://doi.org/10.4155/fmc.11.44

Wilson, K. P., Black, J. A. F., Thomson, J. A., Kim, E. E., Griffith, J. P., Navia, M. A., Livingston, D. J., et al. (1994). Structure and mechanism of interleukin-lβ converting enzyme. Nature, 370(6487), 270. DOI: https://doi.org/10.1038/370270a0

Woodruff, H. B. (2014). Selman A. Waksman, winner of the 1952 Nobel Prize for physiology or medicine. Appl. Environ. Microbiol., 80(1), 2-8. DOI: 10.1128/AEM.01143-13

Woodward, R. B., Au-Yeung, B. W., Balaram, P., Browne, L. J., Ward, D. E., Au-Yeung, B. W., et al. (1981). Asymmetric total synthesis of erythromycin. 2. Synthesis of an erythronolide A lactone system. Journal of the American Chemical Society, 103(11), 3213-3215. DOI: 10.1021/ja00401a050

Xie, J., Okano, A., Pierce, J. G., James, R. C., Stamm, S., Crane, C. M., & Boger, D. L. (2012). Total synthesis of [Ψ [C (□ S) NH] Tpg4] vancomycin aglycon,[Ψ [C (□ NH) NH] Tpg4] vancomycin aglycon, and related key compounds: reengineering vancomycin for dual D-Ala-D-Ala and D-Ala-D-Lac binding. Journal of the American Chemical Society, 134(2), 1284-1297. DOI: 10.1021/ja209937s

Yamaguchi, H., & Miyazaki, M. (2014). Refolding techniques for recovering biologically active recombinant proteins from inclusion bodies. Biomolecules, 4(1), 235-251. DOI: 10.3390/biom4010235

Yang, M., Wu, H., Lian, Y., Li, X., Lai, F., & Zhao, G. (2014). Influence of organic solvents on catalytic behaviors and cell morphology of whole-cell biocatalysts for synthesis of 5′-arabinocytosine laurate. PloS one, 9(8), e104847. DOI: https://doi.org/10.1371/journal.pone.0104847

Yin, W. B., Reinke, A. W., Szilagyi, M., Emri, T., Chiang, Y. M., Keating, A. E., et al. (2013). bZIP transcription factors affecting secondary metabolism, sexual development and stress responses in Aspergillus nidulans. Microbiology, 159(1), 77-88. DOI: 10.1099/mic.0.063370-0

Zheng, H., Hou, J., Zimmerman, M. D., Wlodawer, A., & Minor, W. (2014). The future of crystallography in drug discovery. Expert opinion on drug discovery, 9(2), 125-137. DOI: https://doi.org/10.1517/17460441.2014.872623